A Bidirectional Network for Appetite Control in Larval Zebrafish

***Caroline Lei Wee[1,2,5], *Erin Yue Song[1]**, Robert Evan Johnson[1,2], Deepak Ailani[3], Owen Randlett[1], Jiyoon Kim[1], Maxim Nikitchenko[1], Armin Bahl[1], Chao-Tsung Yang[4], Misha B. Ahrens[4], Koichi Kawakami[3], Florian Engert[1] and **Samuel Kunes[1]**

***Equal contribution first authors**

[1]Department of Molecular and Cell Biology, Harvard University, Cambridge, MA, USA

[2]Program in Neuroscience, Harvard University, Boston, MA, USA

[3]Laboratory of Molecular and Developmental Biology, National Institute of Genetics, Department of Genetics, SOKENDAI (The Graduate University for Advanced Studies), Mishima, Shizuoka, Japan

[4]Howard Hughes Medical Institute, Janelia Farm Research Campus, Ashburn, Virginia, USA.

[5]Current address: Institute of Molecular and Cell Biology, A*STAR, Singapore

ABSTRACT

Medial and lateral hypothalamic loci are known to suppress and enhance appetite, respectively, but the dynamics and functional significance of their interaction have yet to be explored. Here we report that, in larval zebrafish, primarily serotonergic neurons of the ventromedial caudal hypothalamus (cH) become increasingly active during food deprivation, whereas activity in the lateral hypothalamus (LH) is reduced. Exposure to food sensory and consummatory cues reverses the activity patterns of these two nuclei, consistent with their representation of opposing internal hunger states. Baseline activity is restored as food-deprived animals return to satiety via voracious feeding. The antagonistic relationship and functional importance of cH and LH activity patterns were confirmed by targeted stimulation and ablation of cH neurons. Collectively, the data allow us to propose a model in which these hypothalamic nuclei regulate different phases of hunger and satiety and coordinate energy balance via antagonistic control of distinct behavioral outputs.

INTRODUCTION

The regulated intake of food based on caloric needs is a fundamental homeostatically controlled process that is essential for health and survival. The hypothalamus is a highly conserved central convergence point for the neural and biochemical pathways that underlie this regulatory mechanism. Early studies demonstrated by way of electrical stimulation or lesions that specific hypothalamic regions play important roles in the regulation of appetite. For example, while stimulation of ventromedial hypothalamic loci in rodents and cats reduced feeding, activation of more lateral hypothalamic loci increased both hunting behavior and food intake (Anand and Brobeck, 1951; Brobeck et al., 1956; Delgado and Anand, 1953; Krasne, 1962). Conversely, lateral hypothalamic lesions were found to reduce feeding to the point of starvation, whereas medial hypothalamic lesions resulted in overeating (Anand and Brobeck, 1951; Hoebel, 1965; Teitelbaum and Epstein, 1962). Thus, the lateral and medial hypothalamic regions came to be regarded as “hunger” and “satiety” centers, respectively.

Recent experiments employing optical and electrophysiological methods have lent support to these early studies. For example, GABAergic neurons in the lateral hypothalamus were observed to be activated during feeding and essential for enhanced food intake during hunger (Jennings et al., 2015; Stuber and Wise, 2016). However, these experiments have examined only subsets of hypothalamic neurons; their activity patterns and function within the context of the entire network remain unknown. This limited view hampers our understanding of the dynamical interactions between the ensemble of brain circuits thought to be important for the initiation, maintenance and termination of food consumption (Sternson and Eiselt, 2017).

Here, we leverage the small and optically accessible larval zebrafish to identify modulatory regions central to the control of appetite and to shed light on their specific roles and dynamical activity patterns in relation to behavior. Using pERK-based brain-wide activity mapping (Randlett et al., 2015), we first identified neuronal populations that display differential neural activity under conditions that would yield hunger and satiety. We show that lateral and

medial hypothalamic regions have anti-correlated activity patterns during food-deprivation, and voracious or steady state feeding. Next, through a combination of calcium imaging, optogenetics and ablation analysis, we show that a mainly serotonergic neuronal population in the caudal periventricular zone of the medial hypothalamus (cH) are state-dependent regulators of feeding behavior, most likely via their modulation of lateral hypothalamic activity. These results allow us to propose a model where mutually antagonistic brain states regulate energy balance by encoding distinct signals for different facets of appetite control.

RESULTS

Whole brain activity mapping of appetite-regulating regions

Larval zebrafish hunt prey such as paramecia through a sequence of motor actions that has been considered a hardwired reflex response to external prey stimuli (Bianco et al., 2011; Semmelhack et al., 2015; Trivedi and Bollmann, 2013). Only recently has evidence emerged that this behavior is flexibly modulated by satiation state (Filosa et al., 2016; Jordi et al., 2015, 2018) and that larvae at 7 **d**ays **p**ost-**f**ertilization (dpf) display enhanced hunting and enhanced food intake after a period of food-deprivation. A robust readout of food intake in larval zebrafish was obtained both by the ingestion of fluorescently-labeled paramecia and by behavioral analysis, both of which have been adapted for this study (Johnson et al., 2019; Jordi et al., 2015, 2018; Shimada et al., 2012). A 2-hour period of food-deprivation robustly enhances subsequent food intake (Figure 1a). Up to 15 min after the presentation of prey, food-deprived animals display a strong upregulation of hunting and prey intake relative to fish that have continuous access to food (referred to as *fed fish*; Figure 1a), on the basis of fluorescent food ingestion (left panel, Figure 1a) and hunting bouts (right panel, Figure 1a). We refer to this behavior as ‘voracious feeding’. Finally, as the fish consume food, their rate of food intake declines to that of continuously fed fish (Figure 1a). These behaviors likely represent internal states that are commonly referred to as hunger and satiety, and reflect the animal’s underlying

caloric or metabolic needs.

As a first step toward understanding the homeostatic control of feeding in this simple vertebrate system, we employed whole-brain neuronal activity mapping via phosphorylated ERK visualization in post-fixed animals (MAP-mapping; Randlett et al., 2015). Whole brain confocal image datasets of phospho-ERK expression were gathered from animals sacrificed after 15 minutes of voracious feeding that followed a 2-hour period of food deprivation. For comparison, image sets were also gathered from animals that had been fed continuously (*fed fish*). The image volumes were registered to a standardized brain atlas. A difference map (Figure 1b) reveals significant specific differences in neural activity when comparing voracious feeding with continuous feeding (Figure 1b-d, Video 1, Supplementary Tables 1-2). Since both experimental groups experienced the same sensory stimuli (i.e. exposure to paramecia) prior to sacrifice, differences in brain activity should primarily reflect the animals' internal states, which could include manifestations of an altered sensitivity to food cues, activity related to hunting and prey capture, or the motivational history resulting from food deprivation. Indeed, multiple sensorimotor loci related to hunting showed enhanced activity during feeding that followed the food-deprived condition, consistent with the increased feeding behavior observed in food-deprived animals. These loci included the retinal Arborization Fields (AFs; optic tectum and AF7), pretectum, as well as downstream hindbrain loci, such as reticulospinal and oculomotor neurons, all of which are known to be engaged during prey capture behavior (Bianco and Engert, 2015; Muto et al., 2017; Semmelhack et al., 2015). In addition, enhanced activity was observed in the cerebellum, inferior olive, vagal sensory and motor neurons, area postrema and locus coeruleus, areas that have been implicated in producing the corresponding motor output (Ahima and Antwi, 2008; Ammar et al., 2001; Dockray, 2009; Zhu and Wang, 2008).

We focused our attention on brain areas likely to be involved in motivational states related to feeding. These included an area of particularly strong differential activity in the lateral region of the intermediate hypothalamus (Lateral Hypothalamus, LH; Fig. 1b-d), which has

recently been identified as part of the feeding pathway in larval zebrafish (Muto et al., 2017) and whose mammalian analog has been strongly implicated in appetite control (Sternson and Eiselt, 2017). However, the zebrafish LH, unlike its mammalian counterpart, does not harbor melanin-concentrating hormone (MCH)-positive, orexin (hypocretin)-positive neurons, or other major feeding-related peptides (Figure 1- Figure Supplements 1 and 2). We therefore characterized the expression of multiple appetite-related neuromodulators (AgRP, MSH, CART, NPY, MCH, Orexin) and found that they are instead expressed in nearby areas of the hypothalamus (Figure 1 - Figure Supplement 1). The zebrafish LH region does however contain a variety of glutamatergic and GABAergic cell types (Figure 1 - Figure Supplement 2); these non-peptidergic LH cell types that have been shown in rodents to be important for the regulation of feeding (Jennings et al., 2015; Stuber and Wise, 2016).

Among areas that showed relatively decreased neural activity upon feeding food-deprived animals, the most significant was the adjacent caudal hypothalamus (cH), which contains monoaminergic neurons -- mainly serotonergic and dopaminergic cells, with a small fraction of histaminergic cells (Chen et al., 2016; Kaslin and Panula, 2001; Lillesaar, 2011). Indeed, in all of nine independent MAP-mapping experiments, activity was reduced in the cH and increased in the LH within 15 min of food presentation (Fig 1c). The evident inverse relationship between LH and cH neural activity is supported by independent component analysis (Randlett et al., 2015), which was applied to feeding-related MAP-mapping data (Figure 1e, Figure 1 - Figure Supplement 3). Multiple components were uncovered in which cH and LH activities were strongly anti-correlated. These results led us to hypothesize that the lateral and caudal hypothalamic regions form a functionally interconnected network with opposing activity patterns.

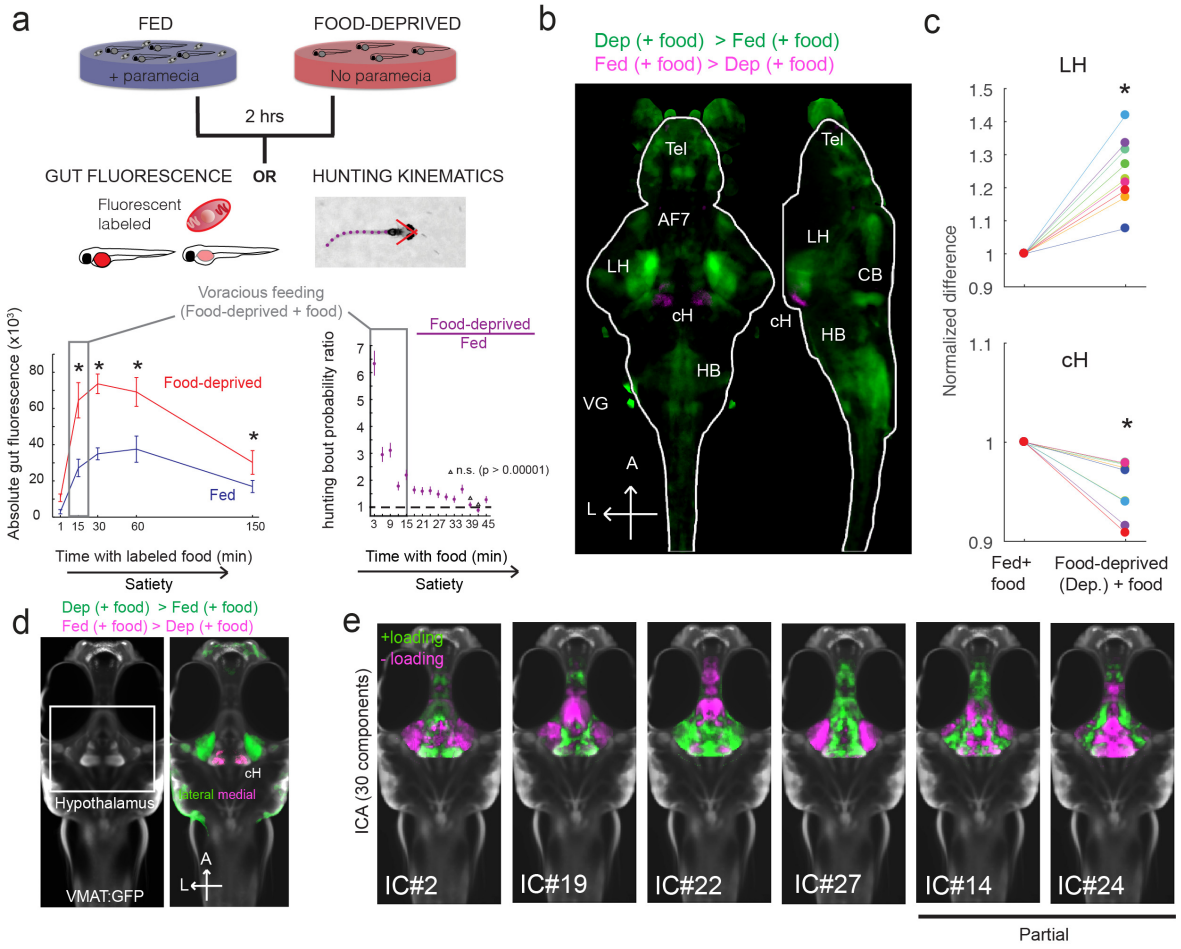

128

Figure 1 with 5 supplements: Whole brain activity mapping reveals anti-correlated hypothalamic regions

(a) Top: The protocols used to quantify feeding behavior in larval zebrafish. At 7 or 8 dpf, larvae were either food-deprived for 2 hours, or fed with excess paramecia for this duration. After 2 hrs (2-4 hours in the case of behavioral imaging), they were subject to a quick wash, followed either by: 1) addition of excess fluorescently-labeled paramecia (left), 2) high-resolution behavioral imaging (right; see Johnson et al., 2019 and methods). Gut fluorescence is both cumulative and diminished by digestion (Jordi et al., 2015) and so lags the dynamics of hunting behavior. **Bottom left:** Gut fluorescence measurements of food-deprived (red) or fed (blue) fish as a function of duration of feeding labeled paramecia. Groups of fed or food-deprived larvae were fixed at the indicated time points (fed: n=7/18/19/17/17 fish, food-deprived: n= 8/23/20/14/15 fish). Food-deprived fish had significantly higher gut fluorescence than fed fish overall ($p = 7.5859x10^{-10}$, Two-way ANOVA, asterisk indicates corrected p-values<0.05. **Bottom right:** The probability of performing a hunting-related swim bout across fed and food-deprived fish groups in 3-minute time bins over 45 minutes. Error bars represent 90% confidence intervals. For all bins except those indicated with triangles, the null hypothesis that initial feeding condition has no effect on hunting-bout probability is rejected ($p < 0.00001$, Fisher's Exact Test comparing binomial probability distributions per bin). Fed: n =85655 bouts from 73 fish; Food-deprived n = 75357 bouts from 57 fish. Since the rate of food intake and hunting behavior was highest in the first 15 minutes (voracious feeding phase, gray boxes), we chose this time point for subsequent MAP-mapping experiments.

(b) Brain-wide activity mapping of food-deprived (Dep.) fish exposed to food for 15 minutes, with subtraction of activity in continuously fed (Fed.) fish. Data from 9 experiments were combined to generate this difference map based on anti-pERK staining fluorescence. Relative activation from feeding after food deprivation yields activated regions including the telencephalon (Tel), Arborization field 7 (AF7), cerebellum (CB), hindbrain (HB), Vagal ganglion (VG) and lateral lobe of the intermediate hypothalamus (LH). Reduced activity was observed in the caudal hypothalamus (cH) and some areas of the telencephalon. Scale bar = 100 μm. Also see Video 1.

(c) ROI-specific pixel intensity analysis of LH and cH regions in 9 independent MAP-mapping experiments (20-30 fish per treatment per experiment). The cH or LH ROI intensities of each individual fish was normalized to the mean cH or LH ROI intensity of all fed fish. Food-deprived fish consistently displayed higher LH and lower cH pERK fluorescence after the onset of feeding ($p=0.0019$ for both cH and LH, one-tailed Wilcoxon signed-rank test).

(d) Z-projection of same MAP-map as described in (**b**) in planes revealing the hypothalamus (right panel), where lateral regions (e.g. lateral hypothalamus, LH) display strong relative activation and medial regions (e.g. caudal hypothalamus, cH) display reduced activity in when food-deprived animals were fed for 15 minutes. The map is overlaid onto a stack for the transgenic line *Tg(etVMAT:GFP)* (left panel) to localize the cH region.

(e) Six examples of independent component analysis (ICA) maps. Voxels for each recovered independent component (IC) are shown as maximum projections, with intensity proportional to the z-score of the loadings of the ICA signal. These ICs, along with others (22/30) highlight LH and cH regions of opposite loadings, suggesting they may be included in a network that displays anti-correlated activity patterns between the cH and LH. A subset of these ICs (e.g. #14 and #24) only showed partial anti-correlation between the cH and the LH. All ICs are shown in Figure 1- Figure Supplement 3. Positive (+) loading and Negative (-) loadings (z-score values of IC signals) are reflected in green and magenta, respectively.

(f) Confocal micrographs of anti-pERK antibody stained brains from animals that were continuously fed (panel (i), left), food-deprived for 2 hours (panel (i), center) and fed for 5 minutes after food-deprivation (panel (i), right). cH (ii) and LH (iii) insets are shown at higher magnification on the bottom and right side respectively. The lateral hypothalamus is shown with subdivisions *lateral lateral hypothalamus* (lLH) and *medial lateral hypothalamus* (mLH). (i) scale bar: 50 μm; (ii) and (iii) scale bar: 20 μm. Fish are mounted ventral side up.

(g) Quantification of cH and LH activities by normalized anti-pERK fluorescence intensity averaging. The normalized anti-pERK staining intensity for each region (ROI) was obtained by dividing the anti-pERK fluorescence from each fish (in all experimental groups) by the average anti-pERK fluorescence for the same ROI of continuously fed fish. Quantitative analysis performed on fish in 6 independent conditions (n =13/11/9/9/13/12). Normalized anti-pERK fluorescence intensity (cH/mLH/lLH): Fed vs Dep. (p = 0.016/0.17/0.17), Dep. vs Dep + 5 min food ($p=3.1x10^{-4}/9.9x10^{-5}/0.02$), Fed vs Dep. + 5 min food (p= 0.0097/0.001/0.08). Asterisks denote $p<0.05$, one-tailed Wilcoxon rank-sum test.
(h) The active cell count metric (bottom panels) was determined as described in Figure 1 - Figure Supplement 4 by a thresholding protocol to isolate and count individual pERK-positive cells within a z-stack. This approach could be reliably performed for areas of sparse active cells (e.g. mLH and lLH) but not where individually labeled pERK-positive neurons are not well separated (such as the cH).
Active Cell count (mLH/lLH): Fed vs Dep. (p = 0.001/0.0038), Dep. vs Dep + 5 min food ($p= 9.7x10^{-5}/1.3x10^{-5}$), Fed vs Dep. + 5 min food (p= 0.0038/0.048). Asterisks denote $p<0.05$, one-tailed Wilcoxon rank-sum test.
(i) Schematic of inferred cH and LH activity in relation to feeding behavior. Note that, based on data in Figure 2, the LH active cell count appears to decline more rapidly than the rise in cH activity (based on cH average fluorescence intensity)

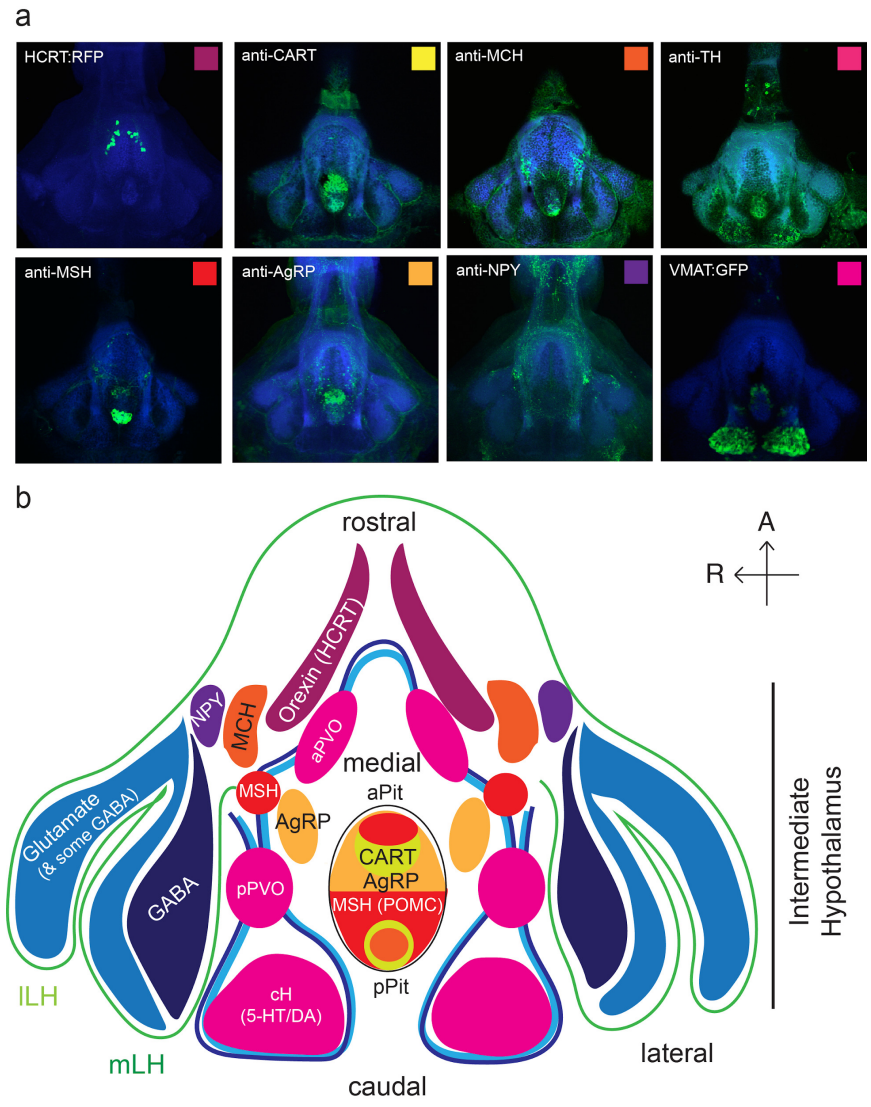

.

Figure 1 - Figure Supplement 1: Anatomical characterization of intermediate hypothalamus expression of appetite related peptides

(a) Expression patterns of a number of feeding-related peptides in the zebrafish hypothalamus, based on antibody-staining or transgenic labels (see Methods). HCRT = hypocretin (orexin), CART = cocaine and amphetamine related transcript MCH = melanin-concentrating hormone, TH = tyrosine hydroxylase (labels dopaminergic and/or noradrenergic neurons), MSH = alpha-melanocyte stimulating hormone, AgRP = Agouti-related peptide, NPY = neuropeptide Y, VMAT = vesicular monoamine transporter (labels dopaminergic (DA) and serotonergic neurons (5-HT)). Note that MCH and HCRT staining is absent from the zebrafish LH. Though not apparent from the schematic, HCRT is located more dorsally. The preoptic area, which contains oxytocinergic as well as other peptidergic neurons, is located more dorsally and not reflected in this schematic.

(b) Schematic view from the ventral perspective summarizing zebrafish hypothalamic peptide expression. GABA (dark blue) and glutamatergic (blue) neurons are found in the lateral hypothalamus (see Figure 1-Figure Supplement 2) and also throughout the medial regions of the hypothalamus. PVO = paraventricular organ, which also contains DA and 5-HT neurons. A number of peptidergic neurons are located within the anterior and posterior pituitary/hypophysis (aPit and pPit). Color code corresponds to images in (a). A = anterior, R = right.

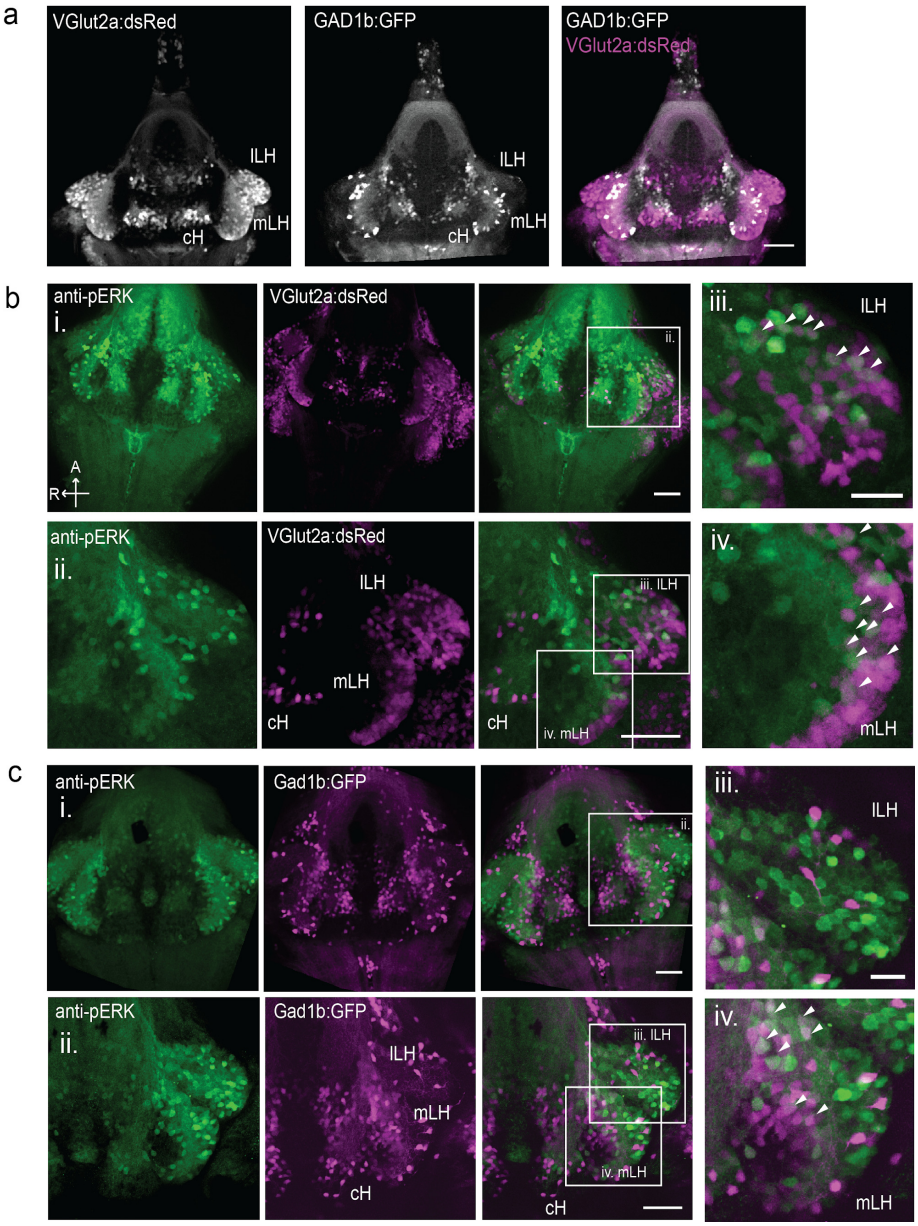

Figure 1- Figure Supplement 2: Characterization of neuronal transmitter types in the zebrafish lateral hypothalamus

(a) Glutamatergic and GABAergic neuron distribution in the hypothalamus. *Tg(VGlut2a:dsRed)* and *Tg(GAD1b:GFP)* transgenic fish were dissected, imaged and registered onto a common reference hypothalamus. All fish in this figure were food-deprived for 2 hours and fixed for analysis after 15 minutes of feeding.

(b) Glutamatergic cells, labeled by *Tg(VGlut2a:dsRed)*, overlap with active (pERK-positive) neurons in both the lLH and outer rim of the mLH. (i) Z-projection of hypothalamus. (ii) Higher magnification images of LH (iii-iv) Inset showing overlap of lLH and outer rim of mLH with glutamatergic cells.

(**c)** GABAergic cells, labeled by *Tg(Gad1b:GFP),* overlap with active neurons in the inner rim of the mLH but not the lLH. (i) Z-projection of hypothalamus. (ii) Higher magnification images of LH showing a subset of z-planes. (iii-iv) Inset showing overlap of inner rim of mLH with GABAergic cells. White arrows point to examples of overlapping cells. All fish were mounted ventral side up. Scale bar (i and ii) = 50 μm. Inset (iii and iv) scale bar = 20 μm.

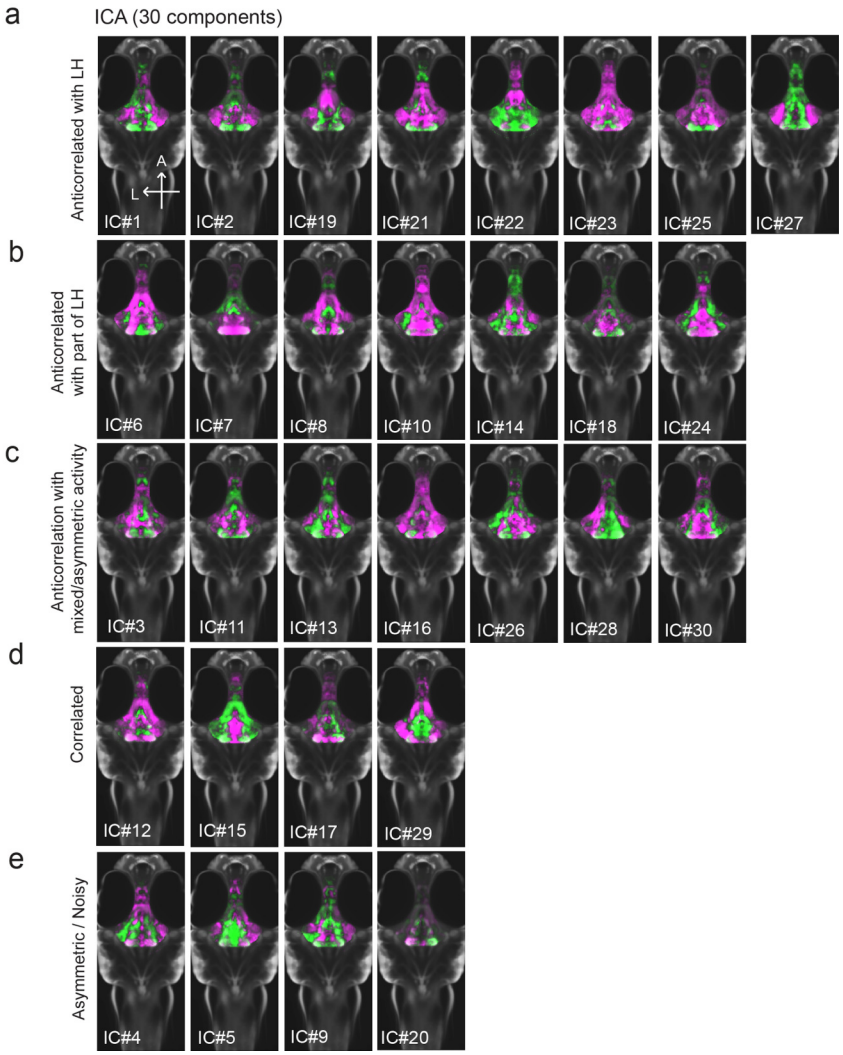

Figure 1- Figure Supplement 3: All 30 independent components extracted from ICA analysis. This method separates pERK signals into statistically independent components based on their correlated and anti-correlated activities, thus identifying putative functional connectivity (both positive or negative relationships) between different brain regions (Randlett et al., 2015; see Methods). Fish included in this analysis were either food-deprived (2 hrs), food-deprived and then fed for 15 minutes prior to harvest, or continuously fed (n = 300 fish total).

(a-c) From this analysis, multiple independent component networks (ICs) were identified in which at least part of the LH displayed an inverse activity relationship (i.e. opposite loadings) with the cH (22/30).

(d) 4/30 ICs had correlated LH and cH activity. However, in these cases lateral loci displayed some anti-correlated activity with medial loci (especially IC #15 and 29).

(e) There were 4/30 ICs that displayed asymmetrical or noisy activity patterns that rendered them unclassifiable.

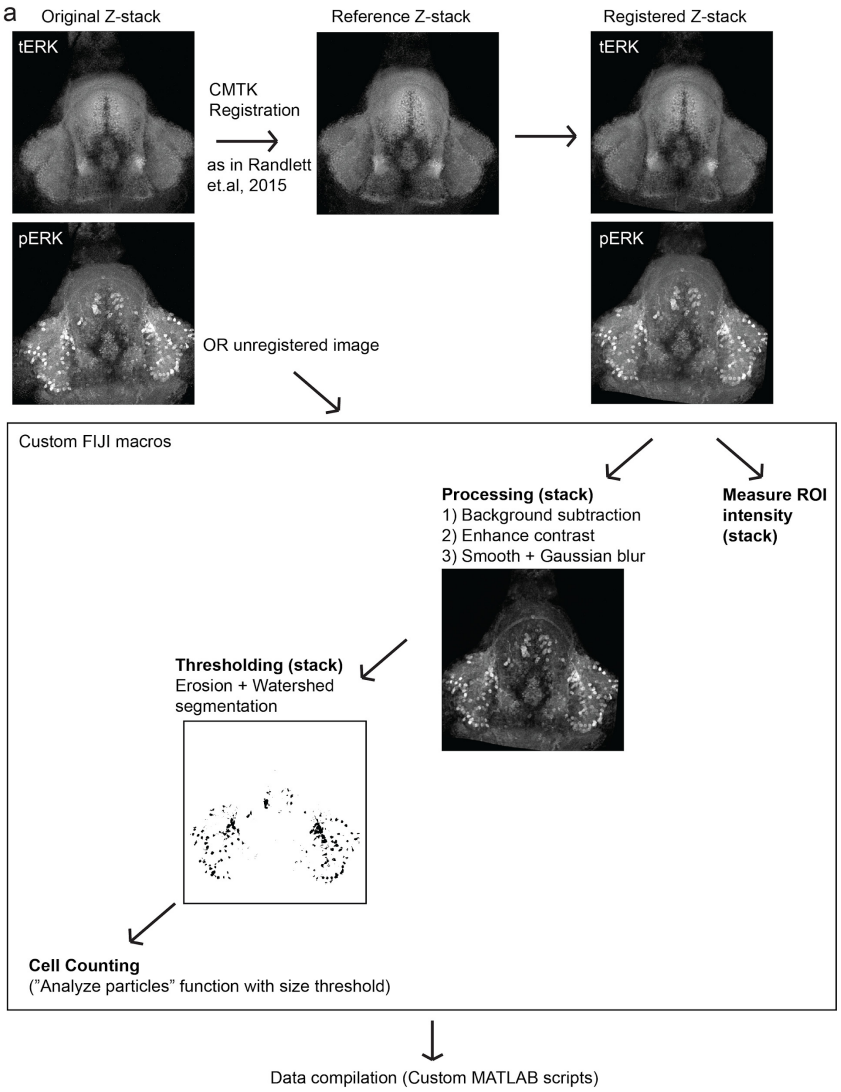

Figure 1 – Figure Supplement 4: Automated quantification of pERK-positive (active) cells

(a) Method by which pERK-positive ("active") cell count were determined in a high-throughput manner. Brain z-stacks obtained from confocal microscopy are registered with a selected reference brain within the same dataset, using the tERK channel, though in experiments where tERK staining was not performed, unregistered images were used (for which individual ROIs have to be defined for each image). A series of processing steps were uniformly applied to segment pERK-positive cells, which were selected using a manually optimized threshold across the entire dataset. Cell counts were obtained using the *Analyze Particles* algorithm within the Fiji software.

Cellular dissection of hypothalamus neural activity reveals modulation by satiation state

To probe these neural activity changes at higher resolution, we performed anti-pERK antibody staining on isolated brains and examined the hypothalamus in time course experiments spanning a period of food-deprivation and subsequent feeding (Figure 1f-h, Figure 2). We quantified the mean anti-pERK fluorescence within a region-of-interest (ROI; Figure 1g, top panels) as well as the number of active cells or cell clusters (Figure 1h; Figure 1 - Figure Supplement 4). These two metrics were employed because the high density of pERK-positive cells in the cH of food-deprived animals made high-throughput quantitation of active cells unreliable, whereas use of this metric in areas of sparse activity (e.g. mLH and LH) yielded better differential sensitivity than ROI averaging. Using these respective metrics, we observed that mean fluorescence in the cH was significantly increased in food-deprived fish, while the number of active neurons in the medial and lateral lobes of the LH (mLH and lLH, respectively) was relatively low (Figure 1f-h). Within the cH, enhanced pERK activity during food-deprivation was most prevalent in serotonergic neurons, but also present in a smaller proportion of dopaminergic neurons (Figure 1 - Figure Supplement 5, Video S2, S3).

During the period of voracious feeding that followed food-deprivation, the pERK-reported activity of cH neurons fell dramatically to a level significantly below that observed in continuously fed fish (Figure 1f-h). This characteristically low cH activity level coincided with a large increase in LH activity, measured by either mean anti-pERK fluorescence or by measurement of the number of individually active neurons, that lasted throughout the period of voracious feeding. Thereafter, as feeding continued at a more moderate pace, and the rate of food ingestion declined, LH neuronal activity likewise declined (especially for lLH neurons; Figure 1h). Reciprocally, cH activity slowly increased back towards baseline levels. After 30 min of feeding, neural activity in both the cH and LH had mostly converged to the baseline level observed for continuously fed fish, consistent with the time course of hunting behavior reduction

(Figure 1a, right panel). Thus these cH and LH populations displayed anti-correlated activity over time frames that spanned a progression of distinct behaviors associated with food-deprivation, voracious feeding and a gradual return to apparent satiety (Figure 1i).

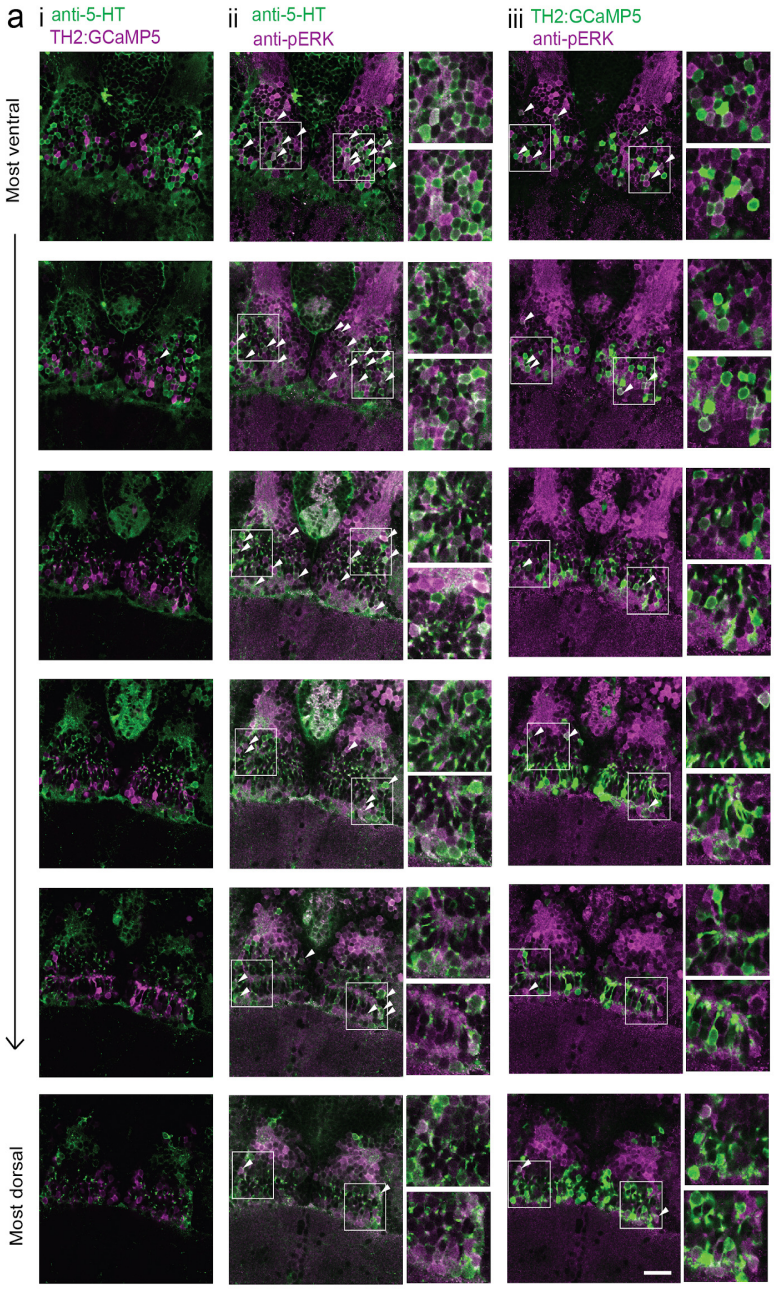

b

Fish	pERK+	5HT+	TH2+	pERK+/5HT+	pERK+/TH2+
1	92	96	110	61	20
2	54	60	63	32	10
3	64	56	86	41	15
4	70	48	91	32	18
MEAN	**70.0**	**65.0**	**87.5**	**41.5**	**15.8**
ERR	**8.04**	**10.63**	**9.67**	**6.84**	**2.17**

% of pERK+ cells that are 5HT+/TH2+		
%5HT+	% TH2+	%unlabeled
66.3%	21.7%	12.0%
59.3%	18.5%	22.2%
64.1%	23.4%	12.5%
45.7%	25.7%	28.6%
58.8%	**22.4%**	**18.8%**
4.61%	**1.52%**	**4.02%**

% of 5HT+/TH2+ that are pERK+	
% of 5HT+	% of TH2+
63.5%	18.2%
53.3%	15.9%
73.2%	17.4%
66.7%	19.8%
64.2%	**17.8%**
4.14%	**0.81%**

Figure 1 - Figure Supplement 5: Food-deprivation induced activity in caudal hypothalamus monoaminergic neurons.
(a) Dopaminergic neurons are labeled in *Tg(TH2:GCaMP5)* fish. These animals were food-deprived for 2 hours and then co-stained with anti-5-HT (to label serotonergic neurons) and anti-pERK antibodies in order to quantify food-deprivation induced activity in both cell types. Each row shows a different z-plane, moving from dorsal to ventral. (i) There is minimal overlap between *Tg(TH2:GCaMP5)*-positive cells (magenta) and 5-HT labeling (green). There is higher overlap of anti-pERK staining (magenta) with (iii) 5-HT-positive cells (green) as compared to (ii) *Tg(TH2:GCaMP5)*-positive cells (green). White arrows point to examples of overlapping cells. White boxes indicate region shown in insets. Scale bar = 20 μm. Full z-stacks for (ii) pERK overlap with anti-5-HT staining (Video 2) and (iii) TH2:GCaMP5 expression (Video 3) are also provided.
(b) Quantification of overlap between pERK-positive cells and anti-5HT staining or *Tg(TH2:GCaMP5)* expression. Other cH cell types, including histaminergic neurons (Chen et al., 2016) are not labeled. Fish 1 corresponds to the fish shown in (a).

Satiation state influences the responses of cH and LH populations to food

To more closely align the activity patterns of cH and LH neuronal populations with feeding behavior, we examined these areas after a 30 minute (i.e. short) or 2-4 hour (i.e. long) period of food-deprivation, with or without a subsequent period of voracious feeding (Figure 2, Figure 2 - Figure Supplement 1). Following food removal, cH activity increased, with an especially large anti-pERK average fluorescence intensity increase after 2 hours of food-deprivation (Figure 2a-b). In contrast to the cH, food removal quickly reduced the frequency of active mLH and lLH neurons (Figure 2a, c). Despite the reduction in LH active cell count over food deprivation, there were no obvious changes in mean LH anti-pERK fluorescence over the course of food-deprivation (Figure 2b). This is because there are few active LH cells in continuously fed and food-deprived fish, thus their overall contribution to the fluorescence average of the mLH and lLH regions of interest is small.

Notably, the addition of prey (paramecia) rapidly reversed the food-deprivation induced patterns of cH and LH neural activity, with an amplitude of change that was correlated with the length of food-deprivation (Figure 2a-c, Figure 2 - Figure Supplement 1d-e). Fish that had been food-deprived for longer periods (2 hrs or 4 hrs) displayed a greater increase in the number of active LH neurons compared to feeding animals that had been food-deprived for only 30 minutes (Figure 2a-c; Figure 2 - Figure Supplement 1d-e). Likewise, the reduction in cH activity

after food presentation was greater when it followed a longer period of prior deprivation (Figure 2a-b; Figure 2 - Figure Supplement 1d). In general, the presence of highly active neurons in the lateral hypothalamus was correlated with food consumption (as measured by gut fluorescence, Figure 2 - Figure Supplement 1a-e).

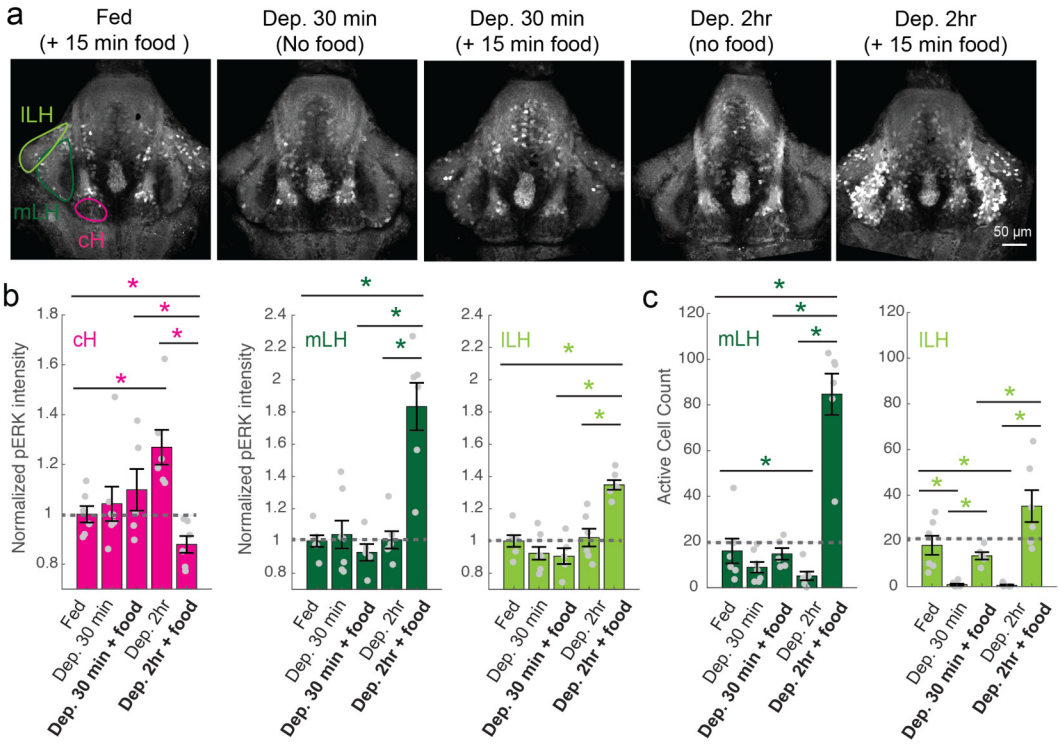

Figure 2 with 1 supplement: cH and LH activities are modulated by food and satiation state
(a) Representative images showing that cH, mLH and lLH activities in the presence and absence of food vary with the extent of food-deprivation (dataset quantified in **b** and **c)**.
(b) Normalized pERK average fluorescence intensity in cH significantly increases with food-deprivation, and is significantly reduced when food is presented to food-deprived fish. Normalized mLH and lLH pERK average fluorescence intensity does not change significantly during food deprivation and strongly increases during voracious feeding (Dep. 2 hr + food). Asterisks denote $p<0.05$. Normalized pERK intensity (cH/mLH/lLH): Fed vs Dep. 30 min ($p = 0.53/0.47/0.15$), Fed vs Dep. 2 hr ($p = 0.0022/0.41/0.59$), Dep. 30 min + food vs Dep. 2 hr + food ($p = 0.041/0.0022/0.0022$), Dep. 30 min vs Dep. 30 min + food ($p = 0.62/0.73/0.62$), Dep. 2 hr vs Dep. 2 hr + food ($p = 0.0022/0.0011/0.0022$), Fed vs Dep. 2 hr + food ($0.047/0.0011/0.0011$). Anti-pERK staining fluorescence was averaged over each entire region of interest (i.e. cH, mLH and lLH; see Methods for details). The normalized anti-pERK staining intensity for each region (ROI) was obtained by dividing the anti-pERK fluorescence from each fish (in all experimental groups) by the average anti-pERK fluorescence for the same ROI of continuously fed fish.
(c) The number of active mLH and lLH cells declines within 30 min of food deprivation, and is significantly enhanced during feeding, particularly after a longer period of food-deprivation. Active cell count (mLH/lLH): Fed vs Dep. 30 min ($p = 0.155/5.8\times10^{-4}$), Fed vs Dep. 2 hr ($p = 0.047/0.011$), Dep. 30 min + food vs Dep. 2 hr + food ($p = 0.0022/0.0043$), Dep. 30 min vs Dep. 30 min + food ($p = 0.07/0.013$), Dep. 2 hr vs Dep. 2 hr + food ($p = 0.0011/0.0011$), Fed vs Dep. 2 hr + food ($p = 0.0022/0.07$), n = 6/7/5/6/6 fish, one-tailed Wilcoxon rank-sum test.

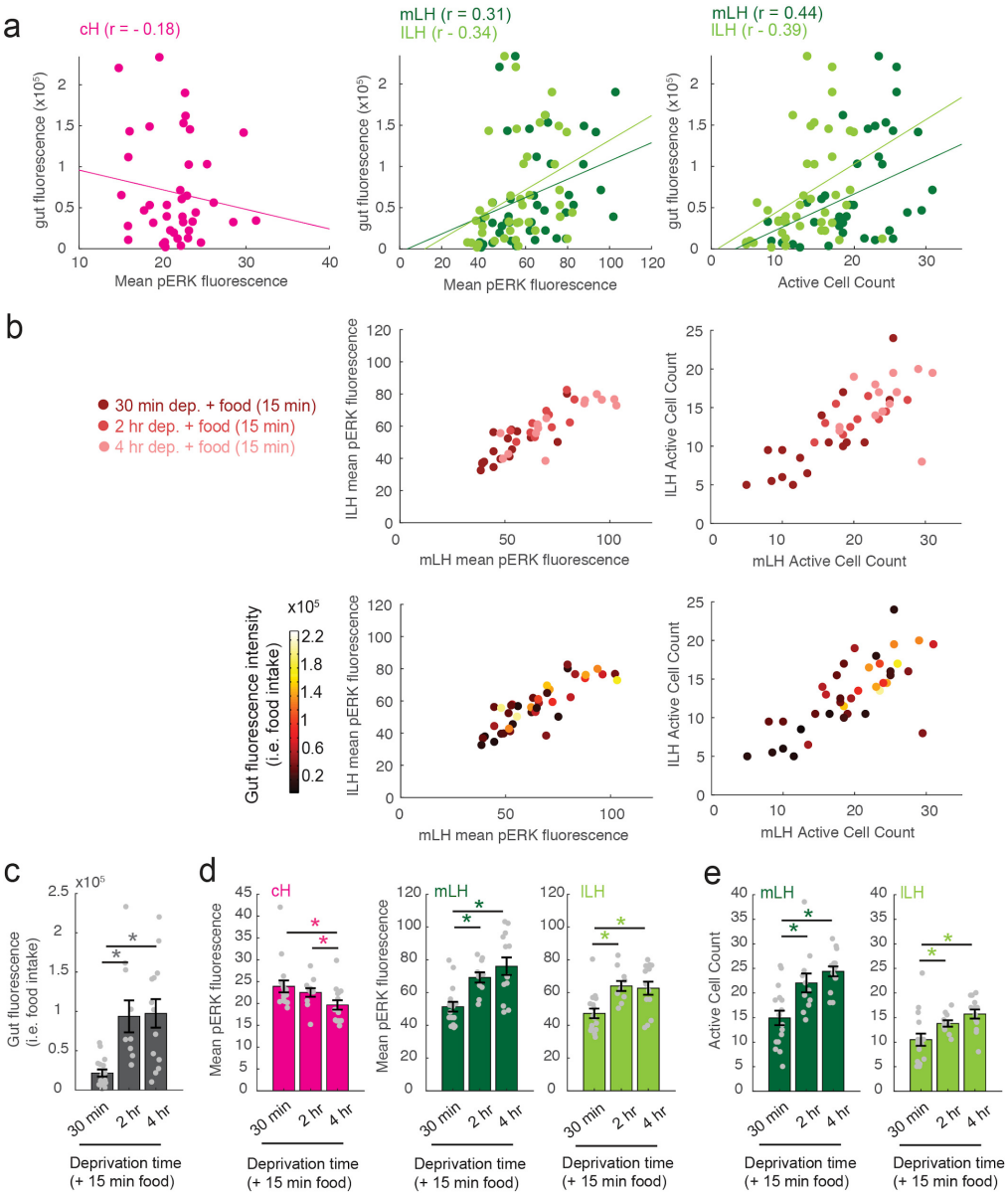

Figure 2 - Figure Supplement 1: Modulation of cH, mLH and lLH activity in relation to feeding. The dataset (n = 41 fish) includes animals food-deprived for 30 min (n = 16), 2 hr (n = 11), or 4 hr (n = 14), and subsequently fed labeled paramecia for 15 min. Brains from these animals were individually-stained with anti-pERK antibody in multi-well plates in order to correlate each one's food intake with cH, mLH and lLH neural activity.

(a) Gut fluorescence (i.e. food intake) of all fish as a function of mean cH pERK fluorescence, mean LH (mLH and lLH) anti-pERK staining average fluorescence and active cell count. Mean pERK fluorescence reflects the average fluorescence within the cH, mLH or lLH regions of interest. This dataset was not normalized. Each datapoint represents an individual fish.

(b) Top: mLH and lLH mean pERK fluorescence (left), and active cell count (right) of all fish (n = 41) plotted as a function of food-deprivation time (denoted by color intensity). **Bottom:** mLH and lLH mean fluorescence (left) and cell count (right) of all fish (n = 41) plotted as a function of gut fluorescence (i.e. food intake) after 15 min of feeding (denoted by color intensity).

(c-e) Quantification of gut fluorescence, cH and LH mean pERK fluorescence and LH active cell count across the different food deprivation times (30 min, 2 hr, and 4 hr). Note that in this dataset, because anti-pERK was conducted on each brain individually, there is higher variance between specimens and reduced statistical significance in cH quantification data (compare with Figure 2b, left panel). Asterisks denote $p<0.05$.
(c) Food intake: After 30 min vs 2 hr deprivation ($p = 2.8x10^{-4}$), 30 min vs 4 hr deprivation ($p = 4.0x10^{-4}$), 2 hr vs 4 hr deprivation ($p = 0.56$). Asterisk denotes $p< 0.05$, n = 16/11/14 fish (30 min/2 hr/4 hr food-deprivation + 15 min food), one-tailed Wilcoxon rank-sum test.
(d) Mean pERK fluorescence (cH/mLH/lLH): After 30 min vs 2 hr deprivation ($p = 0.60/0.001/5.9x10^{-4}$), 30 min vs 4 hr deprivation ($p=0.084/8.6x10^{-4}/0.058$), 2 hr vs 4 hr deprivation ($p =0.02/0.24/0.54$). Sample sizes as in **(c)**.
(e) Active cell count (mLH/lLH): After 30 min vs 2 hr deprivation ($p = 0.0073/0.0094$), 30 min vs 4 hr deprivation ($p= 1.6x10^{-4}/0.0017$), 2 hr vs 4 hr deprivation ($p = 0.056/0.053$). Sample sizes as in **(c)**.

Caudal and lateral hypothalamic responses to food sensory cues are anti-correlated over short timescales

We next set out to characterize acute effects of food sensory cues on both the cH and LH, and also to analyze in more detail the apparent negative activity relationship between these two nuclei. Such analyses require higher temporal resolution than afforded by anti-pERK staining analysis, thus we switched to *in vivo* calcium imaging in cH and LH in live animals (Figure 3). To that end, two transgenic Gal4 drivers, *Tg(116A:Gal4)* and *Tg(76A:Gal4)*, were combined to express GCaMP6s (*Tg(UAS:GCaMP6s)*) in neuronal subsets of both the cH and LH (Figure 3 - Figure Supplements 1-2). The 116A:Gal4 transgene drives expression mainly in serotonergic neurons in the cH (88.9±0.8% 5-HT positive) and paraventricular organ (PVO; Figure 3 - Figure Supplement 1), whereas 76A:Gal4 drives expression in a large proportion of LH cells (Figure 3 - Figure Supplement 2; Muto et al., 2017).

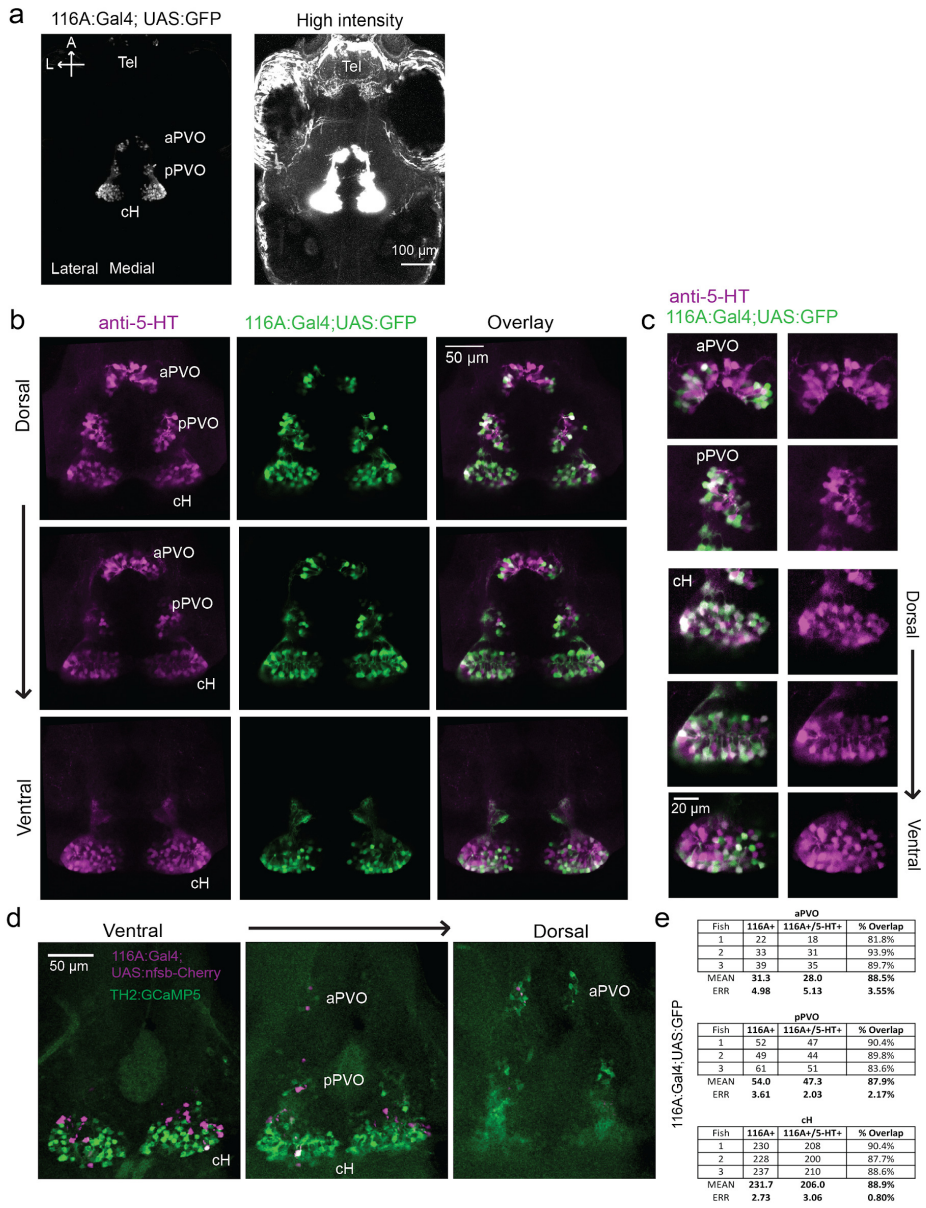

Figure 3 - Figure Supplement 1: Characterization of the 116A:Gal4 line

(a) Z-projection images of whole mount *Tg(116A:Gal4;UAS:GFP)* fish at low (left) and high (right) intensities. Scale bar = 100 µm.

(b) Overlap of *Tg(116A:Gal4;UAS:GFP)* (green) with anti-5-HT (magenta) immunostaining is seen in all layers of the caudal hypothalamus, as well as the anterior and posterior paraventricular organ (aPVO and pPVO). Each row shows a different z-plane, moving from dorsal to ventral. Scale bar = 50 µm.

(c) Higher magnification images of the cH, aPVO and pPVO from left side of image in **(c).**

(d) Minimal overlap of *Tg(116A:Gal4;UAS:nfsb-mCherry)* (magenta) with dopaminergic neurons labeled by *Tg(TH2:GCaMP5)* (green). Note that the *Tg(116A:Gal4;UAS:nfsb-mCherry)* transgenic, which is used in ablation experiments, shows sparser labeling than with *Tg(UAS:GFP).* In this fish, 2 out of 17 (11.8%) of *Tg(116A:Gal4;UAS:nfsb-mCherry)* cells overlapped with *Tg(TH2:GCaMP5) expression*. Scale bar = 50 µm.

(e) Quantification of 5-HT overlap with *Tg(116A:Gal4;UAS:GFP)* in the cH, aPVO and pPVO.

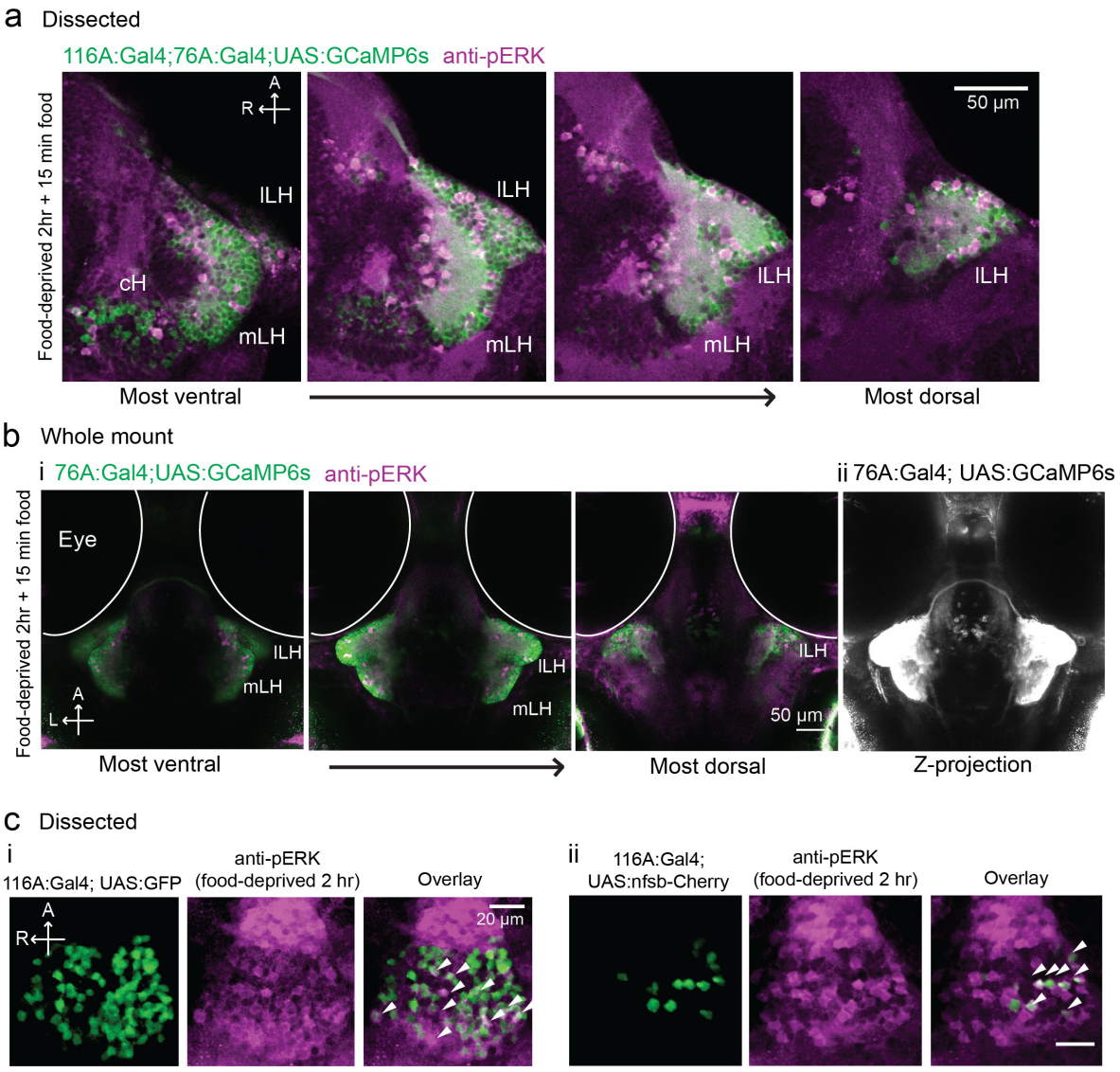

Figure 3 - Figure Supplement 2: Overlap of 116A:Gal4 and 76A:Gal4 driven reporter expression with hypothalamic activity under conditions of food-deprivation and feeding

(a) mLH and lLH activity in voraciously-feeding (food-deprived 2 hr + 15 min paramecia) fish overlaps with *Tg(76A:Gal4;UAS:GCaMP6s)* expression (green, dissected brains). All visible pERK-positive neurons (magenta) were also co-labeled with GCaMP6s. *Tg(116A:Gal4)* is also expressed (green). Scale bar = 50 µm.

(b) mLH and lLH activity in voraciously-feeding fish overlaps with *Tg(76A:Gal4;UAS:GCaMP6s)* expression (whole-mount). All visible pERK-positive neurons were also co-labeled with GFP. Note that more dorsally and anteriorly (as visible in the third panel of (i), and the z-projection in (ii)) other neurons beyond the LH are labeled by *Tg(76A:Gal4;UAS:GCaMP6s)*. Scale bar = 50 µm.

(c) pERK positive cells (magenta) in 2 hr food-deprived fish overlap partially with *Tg(116A:Gal4)* expression (green, dissected brains). (i) Overlap with *Tg(116A:Gal4;UAS:GFP)* (ii) Overlap with *Tg(116A:Gal4;UAS:nfsb-mCherry)*. Scale bar = 20 µm.

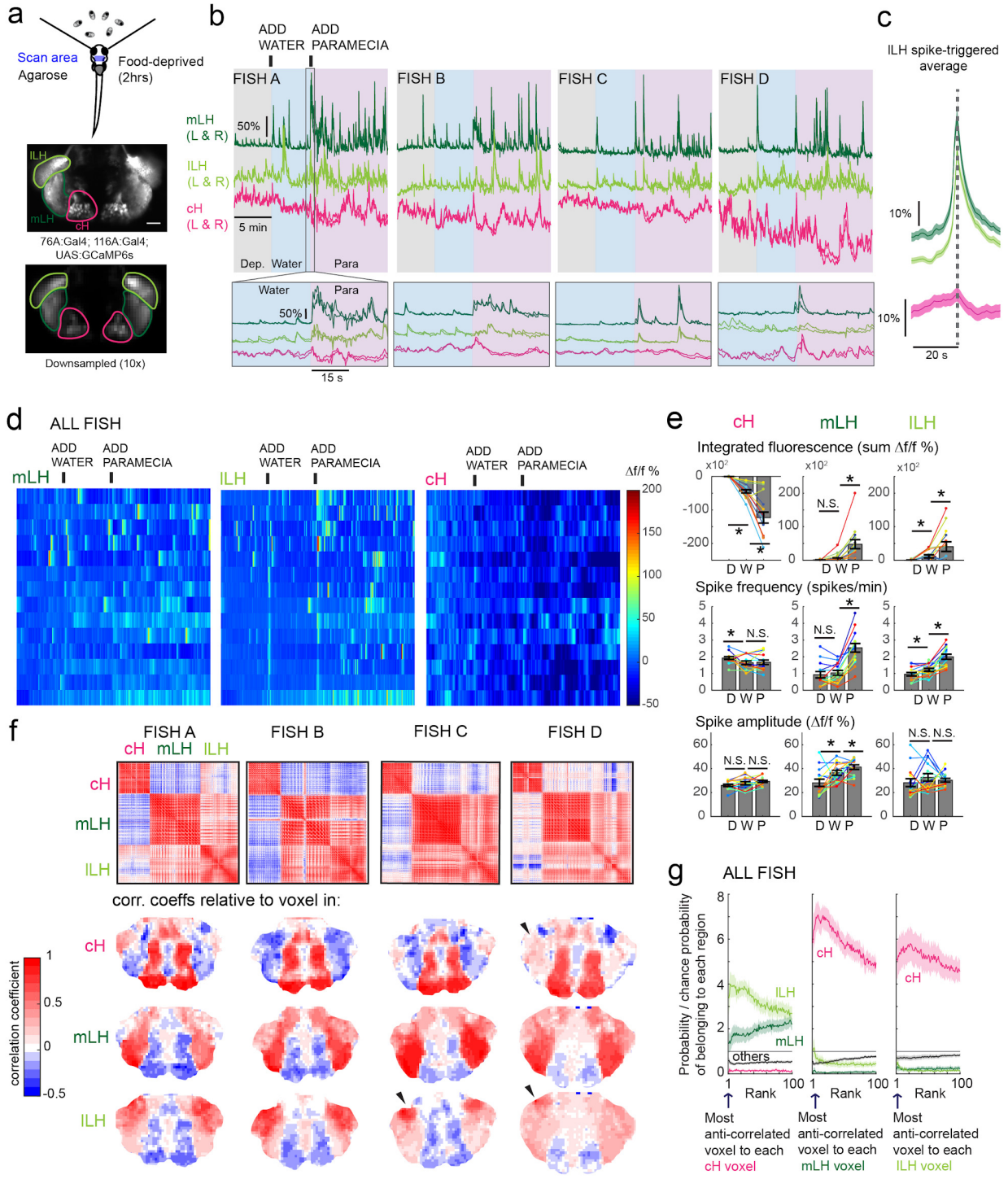

Figure 3 with 3 supplements: Caudal and lateral hypothalamic responses to prey sensory cues are anti-correlated over short timescales

(a) Top: Transgenic fish (2 hr food-deprived) with GCaMP6s expressed in cH and LH neurons were paralyzed, tethered in agarose with their eyes and nostrils free and exposed to live paramecia (prey), as described in Methods. **Top image:** GCaMP expression in the cH and LH driven by two transgenic lines,

Tg(116A:Gal4) and Tg(76A:Gal4) respectively. **Bottom image:** Downsampled image stack used for analysis in (f).

(b) Top: Mean calcium activity (Δf/f) from respective hypothalamic ROIs (shown in (a)) from 4 individual fish during a baseline food-deprived period (Dep.), exposure to water alone (Water), and a dense water drop of paramecia (Para). Traces from left and right hypothalamic lobes of the same animal are overlain, revealing a high degree of correlated activity on opposite sides of the midline. Paramecia presentation increases activity in the LH and reduces activity in the cH, revealing opposing activity on short timescales. **Bottom:** Δf/f traces within area marked by grey box (top), displayed at higher magnification. An increase in LH activity and corresponding reduction in cH activity is observable within seconds of paramecia presentation, except for fish D in which maximal responses only occur after a few minutes (beyond the displayed time window).

(c) Average Δf/f triggered on lLH calcium spikes (left and right lobes averaged) shows a mean corresponding reduction in cH activity (n = 159 lLH spikes extracted from mean Δf/f traces from 14 fish across the entire duration of the experiment).

(d) Raster plots showing mean calcium activity from the hypothalamic lobes (left and right lobes averaged) of 14 fish before and after presentation of water alone and water with paramecia.

(e) Quantification of integrated fluorescence (sum Δf/f %), calcium spike frequency (spikes/min) and calcium spike amplitude (Δf/f %) per fish across experimental epochs (300 s food-deprived baseline (D), 300 s after water (W) delivery or 600 s after paramecia delivery (P). Each colored line represents data from an individual fish (left and right lobes averaged). Water alone was sufficient to significantly reduce cH integrated fluorescence ($p = 6.1 \times 10^{-5}$) and spike frequency (p = 0.0127) but not spike amplitude (p = 0.9324). Water alone was similarly sufficient to increase lLH integrated fluorescence (p = 0.029) and spike frequency (p = 0.0098) but not spike amplitude (p = 0.13). Conversely, water alone was not sufficient to significantly modulate mLH integrated fluorescence (p = 0.48) or spike frequency (p = 0.20), but was sufficient to increase spike amplitude (p = 0.039). Paramecia delivery significantly increased mLH and lLH integrated fluorescence (mLH, $p = 1.2 \times 10^{-4}$; lLH, p =0.045) and spike frequency (mLH, $p = 6.1 \times 10^{-5}$; lLH, 6.1×10^{-4}), while only significantly increasing mLH spike amplitude (mLH, p = 0.045, lLH, p = 0.43), relative to water delivery. In contrast, paramecia delivery significantly reduced cH integrated fluorescence relative to water delivery alone ($p = 3.1 \times 10^{-4}$), but not spike frequency (p = 0.52) nor spike amplitude (p = 0.85). W = water, P = paramecia. Asterisks denote p<0.05, one-tailed Wilcoxon signed-rank test.

(f) Top: Cross-correlogram of hypothalamic cell-sized voxels (cells and/or neuropil from downsampled image stacks, see Figure 3a) from 4 fish. The cH and LH voxels were mostly anti-correlated, whereas voxels within each cluster displayed correlated activity. Black arrowheads indicate region of lLH that appears to be most anti-correlated with the cH. **Bottom:** Correlation coefficients of other hypothalamic voxels relative to a selected voxel with the cH, mLH or lLH. See color key for numerical translation of color maps.

(g) Summary of data from 14 fish, showing the probability of the n^{th} most anti-correlated voxel belonging to each of the other regions (cH, mLH or lLH), normalized to chance probability (gray line) of belonging to each region (i.e. the fraction of all voxels occupied by each region). For example, if we consider all the voxels within the cH, there is a four-fold probability relative to chance of their most anti-correlated voxels (Rank = 1) being part of the lLH.

Using these transgenic animals we examined calcium dynamics in the cH and LH regions in tethered animals during the controlled presentation of prey stimuli (Figure 3a). In these experiments, live paramecia were released in a puff of water in the vicinity of the immobilized fish, which can neither hunt nor ingest prey. Consistent with the results of anti-pERK analysis of post-fixed brains (Figures 1 and 2), activity in the mLH and lLH regions was increased and cH activity quickly reduced, in fact within seconds of paramecia release (Figure 3b, d). Neurons in all three hypothalamic loci also responded to water flow alone, but these responses were significantly less than those elicited by paramecia (Figure 3b, d, e). These prey-induced changes in activity were particularly striking for the mLH region, which displayed both a strongly enhanced spike frequency and spike amplitude upon the introduction of prey. Thus, prey sensory cues, even in the absence of hunting or prey ingestion, strongly and differentially regulate neuronal activity in the caudal and lateral hypothalamus.

The activities of cH and LH neurons also appeared remarkably anti-correlated; both spontaneous or prey-induced fluctuations in one population were accompanied by corresponding opposing activity changes in the other (Figure 3b-c). This observation was supported by cross-correlation analysis between cH, mLH and lLH voxels (Figure 3f), which revealed high correlation within the same hypothalamic region (red color), and anti-correlation between cH and LH regions (blue color). Further, lLH voxels showed more spatial heterogeneity than mLH voxels (Figure 3f), though a small cluster of cells at the most-anterior part of the lLH was most consistently anti-correlated with cH activity (Fish C and D, black arrowheads). When ranked according to their degrees of anti-correlation with voxels from other lobes, the cH and lLH displayed the greatest anti-correlation (Figure 3g). Overall, these results indicate that cH and LH neurons display generally anti-correlated activity over short timescales, in addition to the anti-correlation observed over epochs reflecting motivational states imposed by food deprivation and feeding.

In addition to these studies over short timescales, we also analyzed live imaging traces

that spanned extended time periods (up to 2 hours) of food-deprivation (Figure 3 - Supplement Figure 3). This long-term imaging resulted in some confounding modulation of baseline fluorescence over these timescales (Figure 3 - Figure Supplement 3a, particularly lLH trace), that do not necessarily reflect changes in neural firing (Berridge, 1998; Verkhratsky, 2005) and may well be related to modified internal states caused by tethering and immobilization. Nonetheless, we observed significantly higher calcium spike frequencies and amplitudes in the cH as compared to LH regions over the course of food deprivation (Figure 3 - Figure Supplement 3a, c-d), activity patterns that were the opposite of those observed for these regions when prey was presented (Figure 3b, e). For example, the calcium spike amplitude and frequency of the cH region were many-fold greater than those observed in the mLH region during food-deprivation (Figure 3 - Figure Supplement 3d), whereas after prey presentation, these relative activities were reversed, with the mLH displaying significantly greater spike amplitude and frequency than the cH (Figure 3b, e). Likewise, lLH calcium spike frequency is significantly lower than the cH during food-deprivation, but increases significantly after prey presentation (Figure 3 - Figure Supplement 3d, Figure 3e). Thus, the cH is more active over food-deprivation, and the LH under conditions in which food is present.

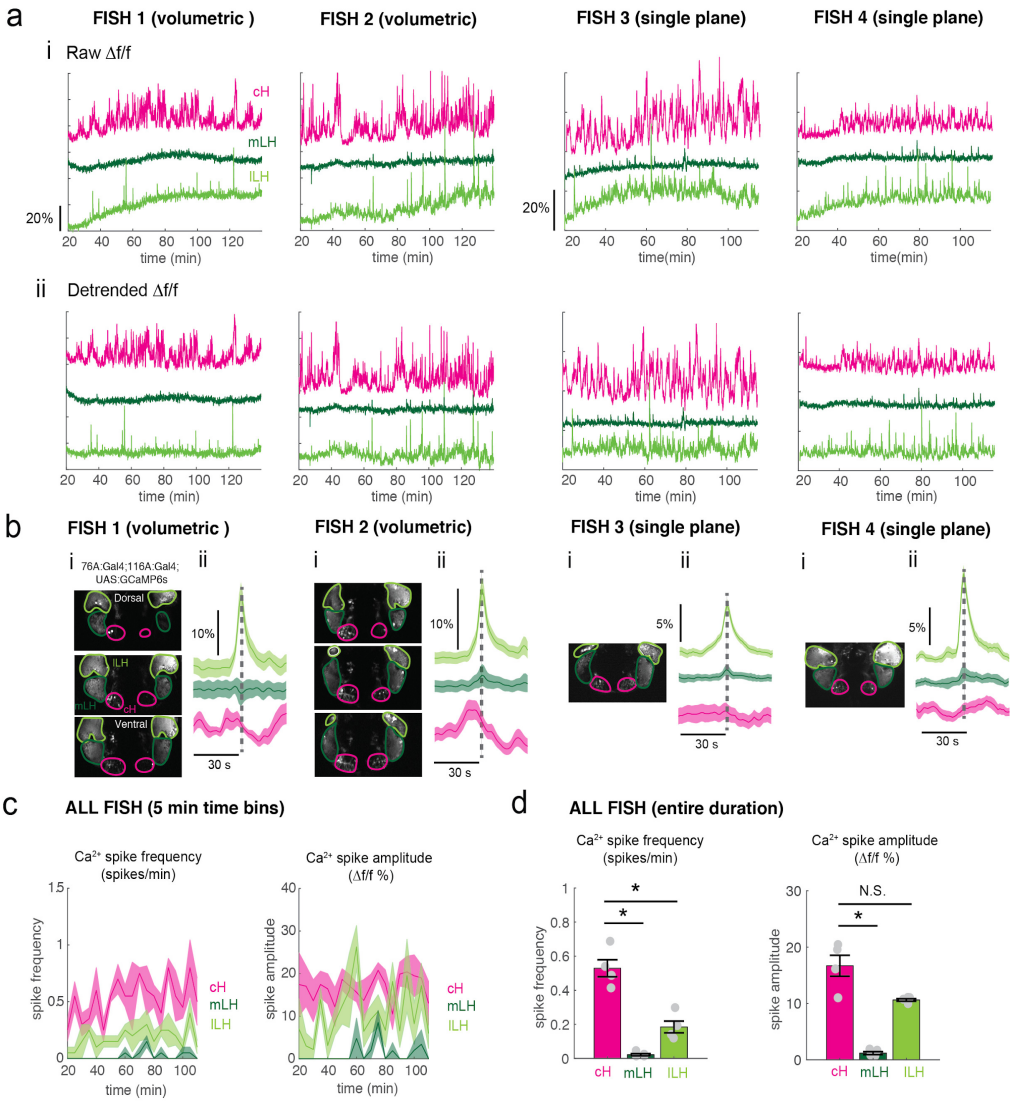

Figure 3 - Figure Supplement 3: Calcium imaging of cH and LH over food-deprivation

Calcium imaging of 4 individual fish during food-deprivation. Note that fish were imaged ~20 min after embedding, thus initial food-deprivation time is already 20 min. Thus, the initial reduction in LH active cell count, which occurs within 30 min (Figure 2) may not be observable using this imaging method.

(a) Fish 1 and 2 were imaged using volumetric imaging for 115 min, whereas fish 3 and 4 were imaged only at a single plane, and for a slightly shorter time period of 90 min (see images in (**b**)) **(i):** Mean Δf/f across the entire (both lobes) of the cH, mLH and lLH (i.e. raw) show increases in baseline fluorescence over time. **(ii)** Mean Δf/f with baseline subtracted (i.e. detrended). Since a rising baseline over long imaging periods is difficult to interpret (see text for discussion), we also display detrended traces.

(b) (i): Average intensity projection images showing imaged regions with ROIs outlined. (**ii)** Spike-triggered averages based on extracted lLH calcium spikes (from detrended traces) usually reveal an accompanying reduction in cH calcium fluorescence (Δf/f).

(c) Calcium spike frequency (spikes/min, left) and calcium spike amplitude (Δf/f %, right) for each ROI averaged over 5 min bins throughout the imaging session for the above 4 fish. Colored lines are the means, shaded areas reflects SEM.

(d) Over the entire imaging period, calcium spike frequency (left) was significantly higher in the cH as compared to the mLH ($p = 0.014$) and lLH ($p = 0.014$). Calcium spike amplitude (right) was also significantly higher in the cH as compared to the mLH ($p = 0.014$), but not the lLH ($p = 0.057$), one-tailed Wilcoxon rank-sum test.

Separation of cH and LH neuronal activities associated with prey detection and ingestion

We next sought to characterize the responses of hypothalamic regions to prey ingestion, as opposed to the mere detection of prey. To distinguish between the consequences of sensory and consummatory inputs, we compared neural activities in food-deprived fish exposed to paramecia or artemia. Artemia are live prey commonly fed to adult zebrafish and are actively hunted by fish at all stages, including larvae (Figure 4a, Video 4). Thus, artemia provide sensory inputs that elicit hunting behavior in larval animals. They are however too large to be swallowed and consumed by larvae. Thus, the comparison between these two types of prey dissociates neural activity triggered by prey detection and hunting from that of food ingestion.

Prey ingestion can only occur in freely behaving animals and thus we needed to return to pERK based activity mapping in post-fixed animals for our analysis. We found that artemia exposure caused significant increases in both mLH and lLH activity, whereas little change was detected in cH neurons (Figure 4a-c). Exposure to paramecia on the other hand triggered an even larger response in both LH lobes and led, as expected, to a significant reduction in cH activity. In order to quantify the relative changes in the mLH and lLH lobes, we compared the artemia-induced activity change (θ_A) to the paramecia-induced activity change (θ_P) for each lobe. The average mLH anti-pERK fluorescence only displayed a marginally greater artemia-induced increase (θ_A/θ_P = 41%) than the lLH region (θ_A/θ_P = 38%; Figure 4c, top panel). However, when the frequency of active neurons was compared, the mLH displayed a much larger response (θ_A/θ_P = 32%) to artemia than the lLH (θ_A/θ_P = 15%). Taken together with our calcium imaging results (Figure 3), these observations indicate that while all three hypothalamic regions (cH, mLH and lLH) are modulated by prey sensory cues, they respond more strongly to prey ingestion. Among these regions, the mLH appears to be the most highly tuned to prey detection in the absence of prey ingestion (Figure 4d).

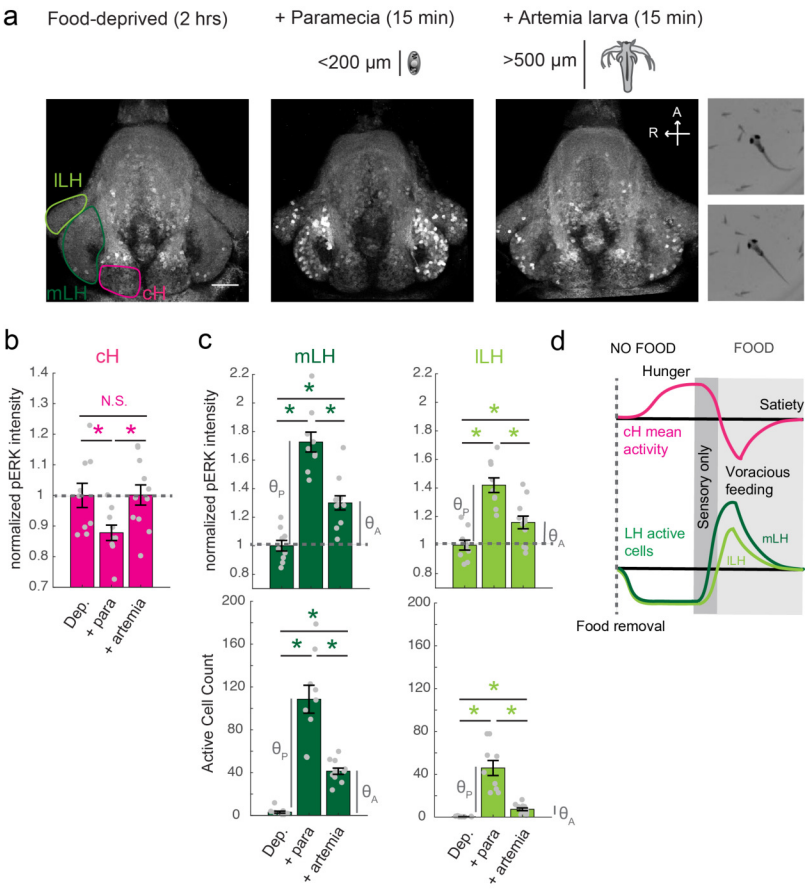

Figure 4: Sensory cues and prey ingestion differentially regulate cH and LH neural activity

(a) Representative images of activity induced by exposure of 7-8 dpf larval zebrafish to paramecia or artemia larvae, as examined by anti-pERK antibody staining. Hatched artemia are actively hunted but are too large to consume, allowing for the dissociation of sensory cues and hunting behavior from prey consumption. Scale bar = 50 µm. Rightmost two panels (top and bottom): Larval zebrafish hunt live artemia, performing J-bends and pursuits with eyes converged (see video 4; Bianco et al., 2011). Asterisks denote $p<0.05$.

(b) cH activity (normalized pERK fluorescence intensity) is significantly reduced by exposure to paramecia but not by exposure to artemia ($p = 0.016$ (paramecia), 0.648 (artemia)).

(c) LH activity can be induced by artemia, and more strongly by paramecia. Both normalized pERK intensity (mLH: $p = 2.06\times10^{-5}$ (paramecia vs control), $p = 7.09\times10^{-4}$ (artemia vs control), $p = 5.43\times10^{-5}$ (artemia vs paramecia); lLH: $p = 2.06 \times 10^{-5}$ (paramecia vs control), $p = 0.020$ (artemia vs control), $p = 0.0019$ (artemia vs paramecia)) and active cell count (mLH: $p = 2.06\times10^{-5}$ (paramecia vs control), $p = 9.58\times10^{-5}$ (artemia vs control), $p = 1.77\times10^{-4}$ (artemia vs paramecia); lLH: $p = 2.06\times10^{-5}$ (paramecia vs control), $p = 9.75\times10^{-5}$ (artemia vs control), $p = 9.86\times10^{-5}$ (artemia vs paramecia)) are shown, with n = 9/9/11 fish, one-tailed Wilcoxon rank-sum test). Anti-pERK staining fluorescence was averaged over each entire region of interest (cH, mLH and lLH; see Methods for details). The normalized anti-pERK staining intensity for each region (ROI) was obtained by dividing the anti-pERK fluorescence from each fish (in all experimental groups) by the average anti-pERK fluorescence for the same ROI of food-deprived (i.e. control) fish. We also compared the artemia-induced activity change (θ_A) to the paramecia-induced activity change (θ_P) for each lobe (see main text).

(d) Differential neural activation of the cH and LH regions in response to prey sensation and hunting as compared to prey ingestion.

590 ***Optogenetic cH activation suppresses lLH neural activity***

591 The observed anti-correlated patterns of caudal and lateral hypothalamus neural activity in both
592 our calcium imaging and pERK-based activity data suggest they might interact via mutual
593 inhibition. For example, during food deprivation, rising cH activity could restrain LH activity,
594 while a subsequent experience of prey detection and ingestion might trigger LH activity that
595 inhibits cH activity. This reduction in cH activity may, in turn, relieve suppression of LH activity, a
596 neural 'switch' that could drive voracious feeding behavior.

597 As an initial test of this hypothesis, we determined whether optogenetic excitation of cH
598 neurons would be sufficient to inhibit LH neural activity. We used the *Tg(y333:Gal4)* line
599 (Marquart et al., 2015) to drive expression of a red-shifted channelrhodopsin (*Tg(UAS:ReaChR-*
600 *RFP)* (Dunn et al., 2016; Lin et al., 2013) in cH neurons (see Figure 5- Figure Supplement 1
601 regarding choice of *Tg(y333:Gal4)*). The *y333:Gal4* line drives ReaChR expression in a large
602 fraction of cH serotonergic neurons (57.4 ± 2.1%; Figure 5- Figure Supplement 1), as well as a
603 smaller fraction of dopaminergic cells (23.9 ± 2.2%; up to 30% overlap observed, Figure 5-
604 Figure Supplement 2). *Tg(HuC:GCaMP6s)* was co-expressed to monitor inhibition of
605 spontaneous LH neuron calcium activity.

606 These tethered transgenic fish were subjected to targeted laser (633 nm) illumination of
607 the cH region to locally activate the ReaChR channel. We found that ReaChR activation in the
608 cH was sufficient to induce cH neural activity (Figure 5a, c). In contrast, ReaChR activation
609 significantly reduced spontaneous lLH calcium spike activity within a 90 second period that
610 followed laser illumination (Figure 5b, d), whereas no significant decrease was observed in mLH
611 activity (Figure 5b, d). Illumination of a control preoptic area region, where *Tg(y333:Gal4)*-
612 driven ReaChR is not expressed, did not affect lLH activity, though we did observe a small
613 increase in mLH activity (Figure 5e). This effect might be visually induced or driven by light-
614 sensitive opsins known to be expressed in the preoptic area (Fernandes et al., 2012). Since no
615 increase was not observed when the cH itself was optogenetically activated, it is plausible that

616 an inhibitory effect of cH stimulation on the mLH is masked by an opposing light response
617 sensitivity. In sum, optogenetic stimulation of cH neural activity is sufficient to inhibit lLH neural
618 activity, consistent with the notion that cH and LH regions interact to modulate the animal's
619 motivational state in response to food deprivation and feeding.

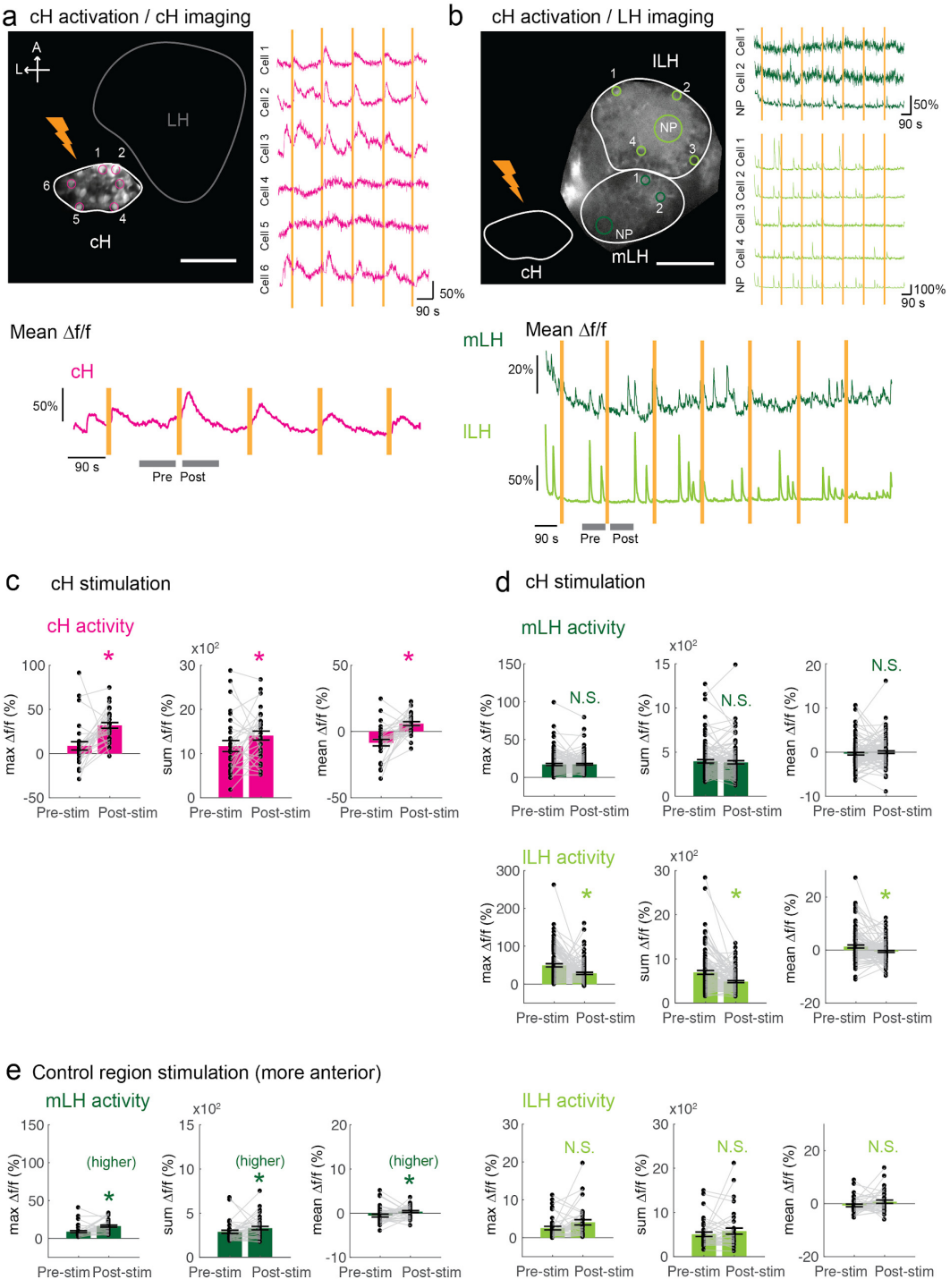

620

Figure 5 with 2 supplements: Optogenetic cH stimulation reduces lLH activity in tethered fish

(a) ReaChR activation of neurons. **Top Panels:** Targeted 633 nm laser illumination(see Methods) of a defined cH area (imaged area) in *Tg(y333:Gal4;UAS:ReaChR-RFP; UAS:GCaMP6s)* fish. These animals express a Tg(*UAS:GCaMP6s)* reporter in the cH under *Tg(y333:Gal4)* control. The animals were subjected to repetitive 10 second laser illumination, with a periodicity of 120 s. Following the 633 nm laser pulses, there is widespread induction of cH activity, as indicated by GCaMP fluorescence (Δf/f) in most regions of interest plotted to the right of the image panel. Scale bar = 50 μm. **Bottom Panel**: Mean Δf/f across the entire outlined cH region versus time. Laser illumination pulses are indicated by orange bars. Gray bars indicate **pre**- and **post**-stimulation periods for which metrics shown in **c-e** were determined.
(b) Inhibition of LH activity by activation of cH neurons in *Tg(y333:Gal4;UAS:ReaChR-RFP; HuC:GCaMP6s)* fish. The animals were subjected to repetitive 10 s laser illumination, with a periodicity of 180 seconds. Laser pulses were delivered to the cH (orange lightning symbol) as in **a**, and calcium imaging was recorded from the indicated LH areas (white outlines). Region of interest traces are shown to the right of the image panel for the indicated areas (**cells** and neuropil (**NP**)). There is an apparent reduction of spontaneous lLH GCaMP fluorescence spikes in the post-stimulation period. Scale bar = 50 μm. Bottom: Mean Δf/f across mLH and lLH ROIs over time.
(c-e) Comparison of mean, summed and maximum Δf/f metrics for 90 s window before and after ReaChR stimulation (gray bars in bottom panels in **a** and **b**). Each data point represents a single stimulation event, like those shown in **a** and **b**. Asterisks denote $p<0.05$.
(c) cH activity increases after illumination of *Tg(y333:Gal4; ReaChR:RFP)*-positive cH neurons, n= 29 illuminations across 8 fish, p = 0.0002 (max Δf/f) / 0.036 (sum Δf/f) / 9.2×10^{-5} (mean Δf/f), one-tailed Wilcoxon signed-rank test.
(d) lLH activity is inhibited (p = 0.0003 (max Δf/f) /1.8×10^{-6} (sum Δf/f) / 0.049 (mean Δf/f)), whereas mLH activity appears unchanged after after illumination of *Tg(y333:Gal4; ReaChR:RFP)*-positive cH neurons (p = 0.74 (max Δf/f) / 0.85 (sum Δf/f) / 0.13 (mean Δf/f)), n = 108 stimulations across 9 fish, two-tailed Wilcoxon signed-rank test.
(e) Illumination of a control preoptic region (outside of the area labeled by *Tg(y333:Gal4; ReaChR:RFP)* expression) resulted in a small increase in mLH activity (p = 0.0003 (max Δf/f) / 0.039 (sum Δf/f) /0.039 (mean Δf/f) and no change lLH activity (p = 0.099 (max Δf/f) / 0.65 (sum Δf/f) / 0.096 (mean Δf/f), n = 37 stimulations from 5 fish, two-tailed Wilcoxon signed-rank test.

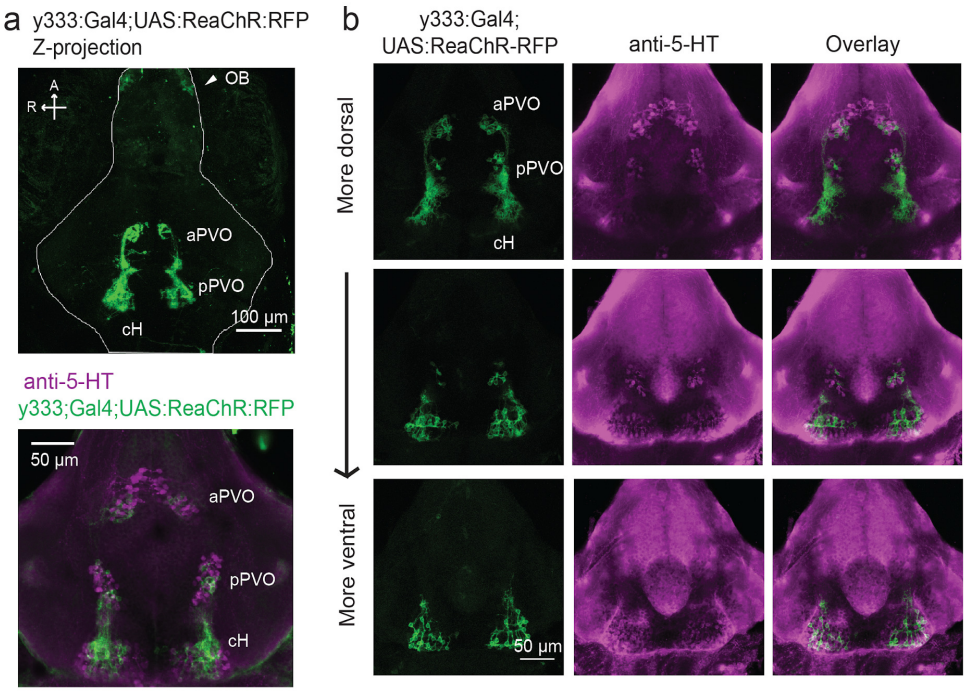

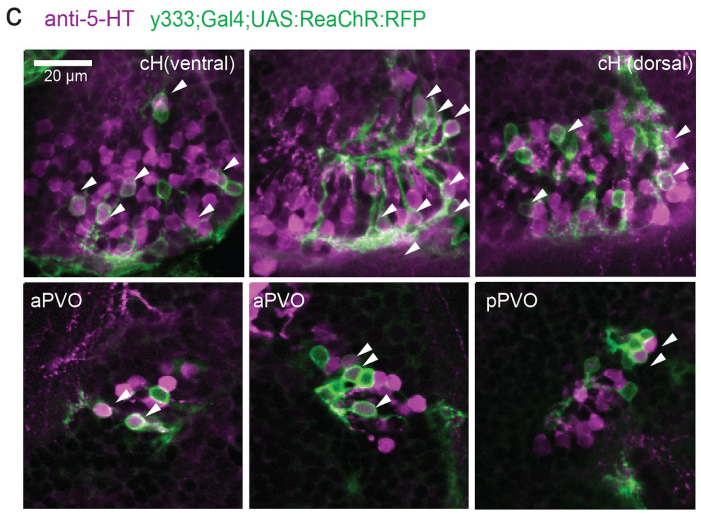

d

y333:Gal4;UAS:ReaChR-RFP

aPVO

Fish	y333+	y333+/5-HT+	% Overlap
1	12	7	58.3%
2	35	20	57.1%
3	19	10	52.6%
4	16	8	50.0%
MEAN	**20.5**	**11.3**	**54.5%**
ERR	**5.04**	**2.98**	**1.95%**

pPVO

Fish	y333+	y333+/5-HT+	% Overlap
1	13	6	46.2%
2	29	15	51.7%
3	20	9	45.0%
4	19	9	47.4%
MEAN	**20.3**	**9.8**	**47.6%**
ERR	**3.30**	**1.89**	**1.47%**

cH

Fish	y333+	y333+/5-HT+	% Overlap
1	44	26	59.1%
2	87	54	62.1%
3	50	28	56.0%
4	59	31	52.5%
MEAN	**60.0**	**34.8**	**57.4%**
ERR	**9.51**	**6.50**	**2.05%**

Figure 5- Figure Supplement 1: Serotonergic identity of y333:Gal4-positive neurons

(a) We used an alternative cH-labeling Gal4 line, *Tg(y333:Gal4)* (Marquat et al.,2015) to drive *Tg(UAS:ReaChR-RFP)* expression, as we were unable to detect any *Tg(116A:Gal4)* driven ReaChR expression on the basis of its Red Fluorescent Protein tag. **Top:** Whole mount confocal z-stack of a *Tg(y333:Gal4;UAS:ReaChR-RFP)* (green) shows relatively specific expression in the caudal hypothalamus, as well as some labeling in the olfactory bulb (white arrow) and other scattered cells. Scale bar = 100 µm. A = anterior, R = right. **Bottom:** Z-projection image of an isolated anti-5-HT (magenta) stained brain mounted ventral side up. Scale bar = 50 µm.

(b) Overlap of *Tg(y333:Gal4;UAS:ReaChR-RFP)* (green) with anti-5-HT immunostaining (magenta) visible in all layers of the caudal hypothalamus. There is also a lower amount of overlapping expression in the

paraventricular organ (PVO). Each row displays a different Z-plane, from dorsal (top) to ventral. Brains are mounted ventral side up. Scale bar = 50 µm.
(c) Higher magnification view showing moderate overlap of *Tg(y333:Gal4;UAS:ReaChR-RFP)* with anti-5-HT staining in the cH and PVO. Arrows indicate cells with overlapping RFP and 5-HT expression. Scale bar = 20 µm.
(d) Quantification of overlap between 5-HT and *Tg(y333Gal4;UAS:ReaChR-RFP)* expression in the cH and PVO.

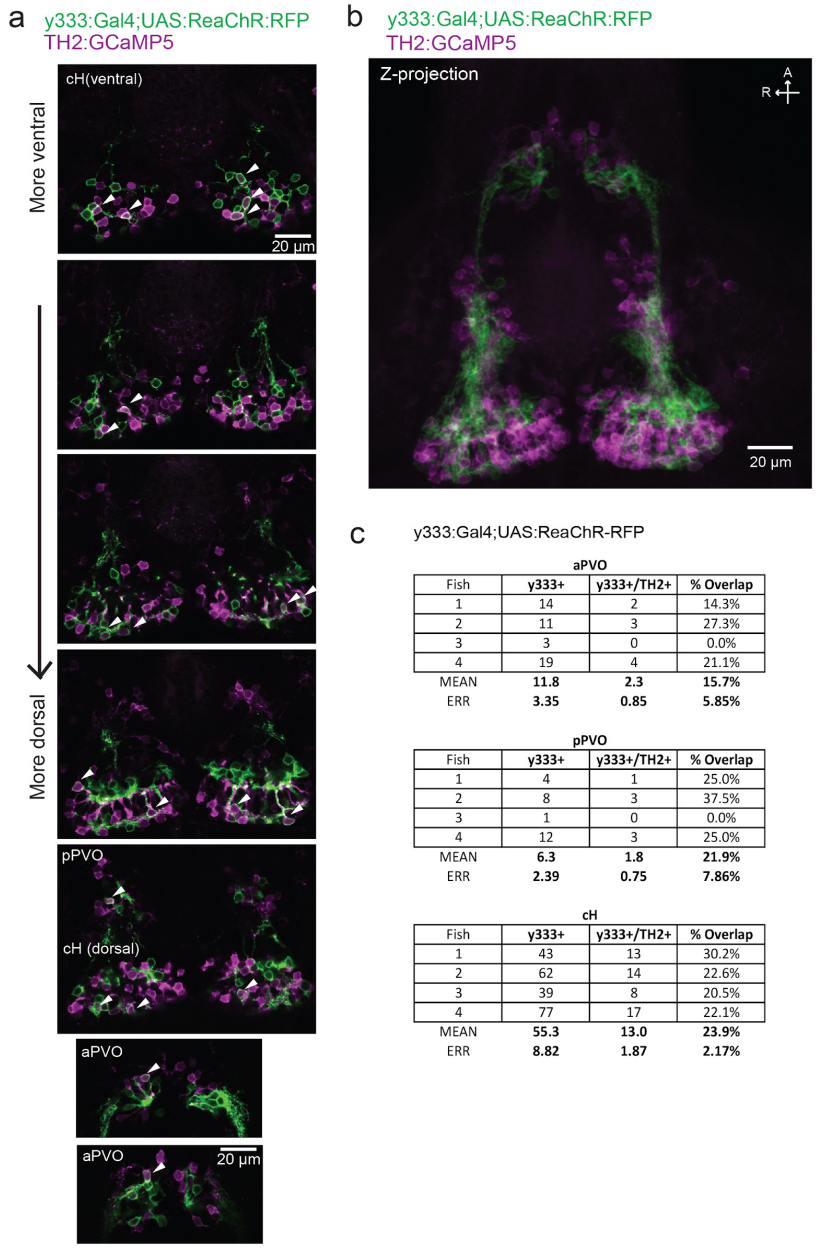

c

y333:Gal4;UAS:ReaChR-RFP

aPVO

Fish	y333+	y333+/TH2+	% Overlap
1	14	2	14.3%
2	11	3	27.3%
3	3	0	0.0%
4	19	4	21.1%
MEAN	**11.8**	**2.3**	**15.7%**
ERR	**3.35**	**0.85**	**5.85%**

pPVO

Fish	y333+	y333+/TH2+	% Overlap
1	4	1	25.0%
2	8	3	37.5%
3	1	0	0.0%
4	12	3	25.0%
MEAN	**6.3**	**1.8**	**21.9%**
ERR	**2.39**	**0.75**	**7.86%**

cH

Fish	y333+	y333+/TH2+	% Overlap
1	43	13	30.2%
2	62	14	22.6%
3	39	8	20.5%
4	77	17	22.1%
MEAN	**55.3**	**13.0**	**23.9%**
ERR	**8.82**	**1.87**	**2.17%**

Figure 5- Figure Supplement 2: Characterization of dopaminergic identity of y333:Gal4 line
The *Tg(y333:Gal4; UAS:ReaChR-RFP)* line (green) was crossed to *Tg(TH2:GCaMP5)* (magenta) to quantify the overlap of *Tg*(*y333:Gal4)* with dopaminergic (TH2-positive) cells.
(a) High magnification image showing moderate overlap of *Tg(y333:Gal4;UAS:ReaChR-RFP)* (green) with TH2-expressing cells (magenta) in the cH and PVO. Arrows indicate cells with overlapping RFP and

TH2 expression. Scale bar = 20 μm. A = anterior, R = right.
(b) Z-projection image of the same brain shown in **(a),** with *Tg(TH2:GCaMP5)* expression shown in magenta. Scale bar = 50 μm.
(c) Quantification of overlap between *Tg(TH2:GCaMP5)* and *Tg(y333Gal4;UAS:ReaChR-RFP)* expression in the cH and PVO.

Functional dissection of the role of cH serotonergic neurons in feeding behavior

The opposing patterns of cH and LH activity suggest they might encode opposing functions in the motivation and control of feeding behavior. Increased cH activity during food deprivation might encode a motivated state that leads to enhanced prey detection, enhanced hunting behavior and increased prey ingestion. In contrast, the incremental increase in cH activity during feeding (Figure 1g) might progressively inhibit ILH activity (Figure 5) and thus inhibit prey ingestion (Muto et al., 2017). To test these expectations, we used optogenetic ReaChR activation to increase cH neuron activity during food deprivation or during voracious feeding. We reasoned that since after a short period of food deprivation, cH activity is relatively low (Figure 2a, b), optogenetic cH neuron activation in such animals would mimic a longer food deprivation and yield subsequent voracious feeding. In contrast, animals that are already feeding voraciously will have very low cH activity (Figures 1f-g, 2a-b); cH activation in these animals might thus reduce voracious feeding by mimicking the 'satiated' state (Figure 1f, g).

Accordingly, animals expressing ReaChR in cH neurons (*Tg(y333:Gal4), Tg(UAS:ReaChR-RFP)*) were exposed to 630 nm illumination and assessed for ingestion of fluorescently labeled paramecia (Figure 6). Such animals exhibited enhanced cH activity following illumination (Figure 6- Figure 6 Supplement 1). As expected, animals that had been illuminated during a short period of food-deprivation subsequently consumed significantly more paramecia than control fish, which were similarly food-deprived and illuminated, but lacked the ReaChR transgene (Figure 6a). In contrast, fish that had been illuminated at the end of a two-hour food-deprivation period displayed a high level of prey ingestion irrespective of whether the ReaChR channel was present. Thus, the high level of cH activity produced by two hours long

705 food deprivation could not be augmented by optogenetic activation.

706 On the other hand, when cH activity was optogenetically excited during voracious
707 feeding (where cH activity would normally be very low), the animal's prey ingestion was reduced
708 (Figure 6b). We presume that increased cH activity inhibits lLH activity (Figure 5), which in turn
709 is associated with satiation and lack of feeding (Figure 1f, g). Indeed, such inhibition of lLH
710 signaling has been shown to reduce prey capture success in comparable studies (Muto et al,
711 2017).

712 Finally, we asked what would happen if cH activity was reduced by partial ablation of
713 serotonergic cells. Chemical-genetic ablation was performed via expression of a transgenic
714 bacterial nitroreductase (*Tg(UAS:nfsb-Cherry)* (Curado et al., 2008; Davison et al., 2007;
715 Pisharath and Parsons, 2009) that was driven in cH serotonergic neurons by *Tg(116A:Gal4)*
716 (Figure 2- Figure Supplement 2). Animals treated with the chemical MTZ displayed a loss of
717 neurons that express nfsb-mCherry (Figure 6 - Figure Supplement 2). These animals were
718 compared in prey ingestion to sibling control animals lacking the *Tg(UAS:nfsb-Cherry)*
719 transgene (Figure 6c). Fish with ablated cH serotonergic neurons displayed greater food
720 ingestion than control animals irrespective of whether the animals had been food-deprived or
721 continuously fed (Figure 6c). Animals that had been continuously fed displayed greater prey
722 ingestion when fluorescently tagged prey were ingested. They thus would appear to display a
723 defect in cH mediated inhibition of feeding (Figure 6b) that could underlie satiety. Animals that
724 had been food deprived and given fluorescently tagged paramecia displayed greater than
725 normal (relative to non-ablated control animals) voracious feeding (Figure 6c). Taken together,
726 these results are consistent with the notion that cH activity regulates hunting and prey ingestion,
727 at least partially via inhibition of hunting and prey ingestion behaviors.

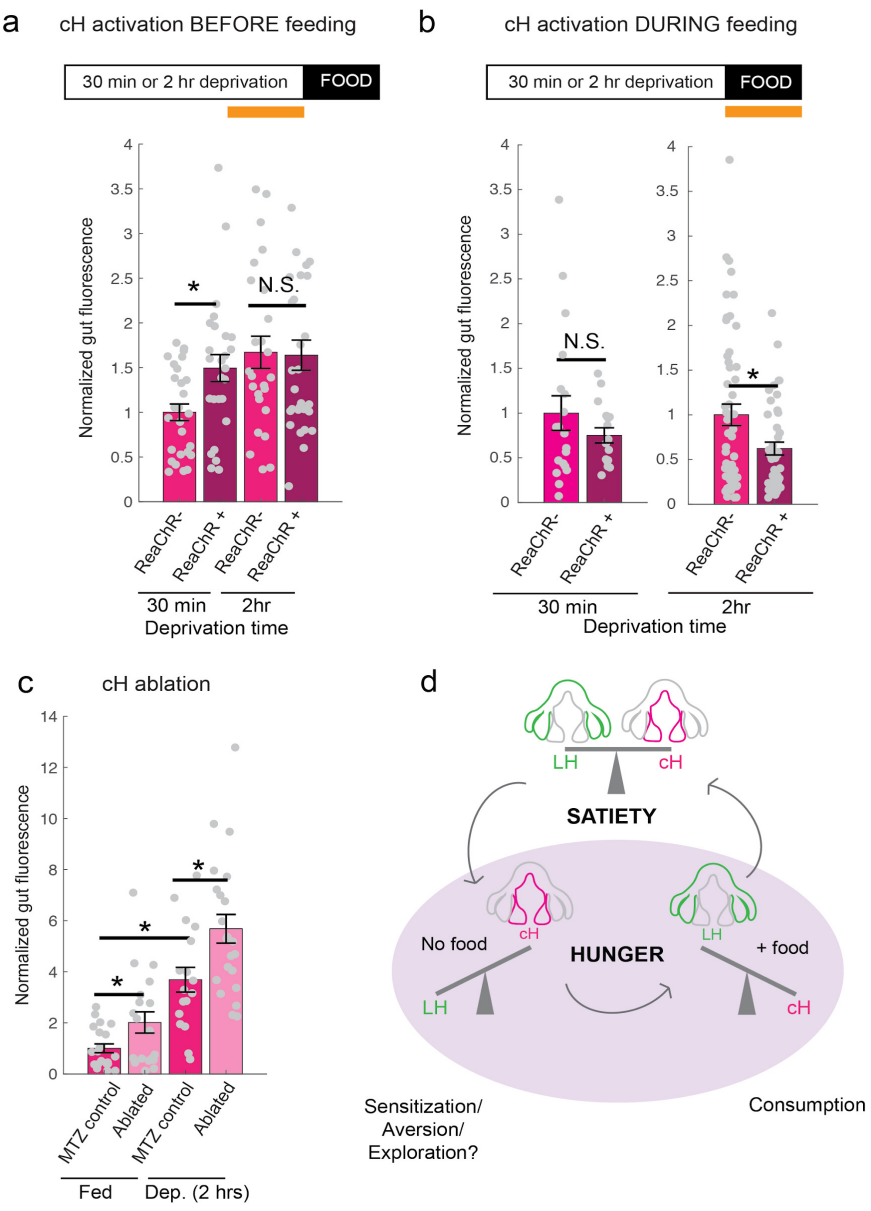

Figure 6 with 2 supplements: Role of the cH in behavioral control

(a) Animals expressing the ReaChR transgene *Tg(UAS:ReaChR-RFP)* under control of the (*Tg(y333:Gal4)* driver were exposed to 630 nm illumination (orange bar in schematic) for 10 minutes prior to feeding and assessed for subsequent ingestion of fluorescently labeled paramecia. *Tg(y333:Gal4; UAS:ReaChR-RFP)* stimulation increased food intake in 30 min food-deprived but not 2 hr food-deprived fish, during subsequent food presentation. Dep. (30 min): n = 27/26 (ReaChR-/ReaChR+), p = 0.005. Dep. (2 hr): n = 25/29 (ReaChR-/ReaChR+), p = 0.36, one-tailed Wilcoxon rank-sum test. Asterisks denote p<0.05. Since ReaChR expression via 116A:Gal4 was negligible, we used another Gal4 (*Tg(y333:Gal4)*) line that is also specific to the cH when ReaChR is expressed. Fed and food-deprived fish were assayed simultaneously, thus all results were normalized to fed controls. ReaChR- controls do not have visible *Tg(y333:Gal4;UAS:ReaChR-RFP)* expression, and thus are a mixture of siblings expressing *Tg(y333:Gal4) only*, *Tg(UAS:ReaChR-RFP)* or neither of these transgenes, each with ⅓ probability.

(b) Left: Optogenetic activation of *Tg(y333:Gal4; UAS:ReaChR-RFP)* fish (orange bar in schematic) during feeding in fish that were food-deprived for 30 min does not significantly reduce food intake: n = 19/16 (ReaChR-/ReaChR+), p = 0.44 (N.S.); **Right:** Optogenetic activation of *Tg(y333:Gal4; UAS:ReaChR-RFP)* fish during feeding in 2 hr food-deprived fish reduces food intake: n = 53/44 (ReaChR-/ReaChR+), p = 0.042. Since 30 min and 2 hr food-deprived fish were assayed in different experiments, gut fluorescence normalized to their respective controls, one-tailed Wilcoxon rank-sum test.
(c) Nitroreductase-mediated ablation of the cH in (*Tg(116A:Gal4;UAS-nfsb:mCherry)* or negative fish treated with metronidazole (MTZ) from 5-7 dpf significantly enhances food intake in 8 dpf fish. p = 0.0042/0.041/1.38x10^{-5} (fed control vs fed ablated, 2 hr deprived control vs 2 hour deprived ablated, fed vs 2 hr deprived), n = 29 (fed control) /28 (fed ablated) /22 (dep. control) /29 (dep. ablated), two-tailed Wilcoxon rank-sum test. Controls do not have visible *Tg(116A:Gal4;UAS:nfsb-mcherry)* expression, and thus are a mixture of siblings expressing *Tg(116A:Gal4) only*, *Tg(UAS:nfsb-mcherry)* or neither of these transgenes, each with ⅓ probability.
(d) Schematic summarizing our results. We propose distinct roles of the cH during hunger, depending on the presence or absence of food. See Supplementary File 1 – Conceptual Circuit Model for elaboration.

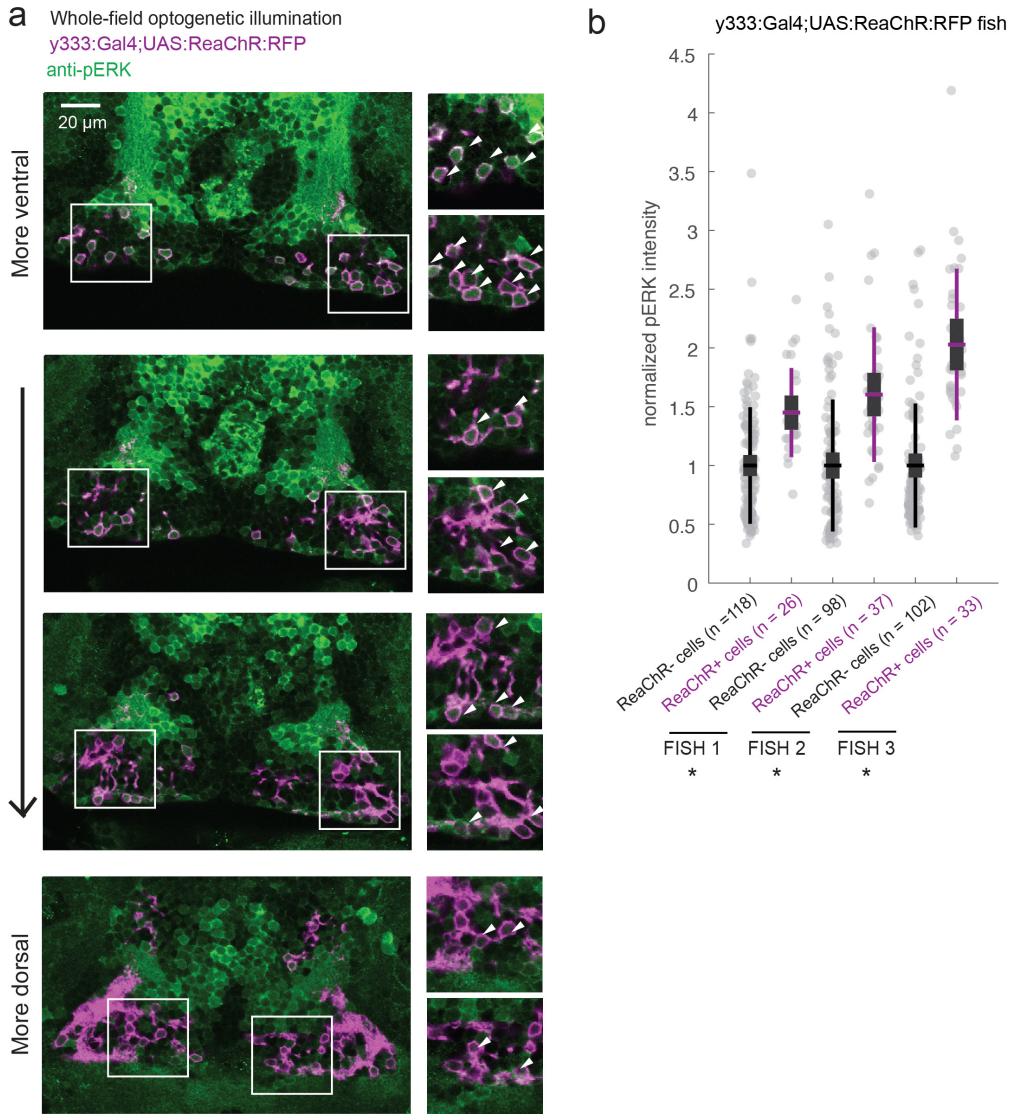

Figure 6 – Figure Supplement 1: ReaChR activation by whole-field optogenetic illumination

(a) *Tg(y333:Gal4;UAS:ReaChR-RFP) (magenta)* optogenetic stimulation during feeding is sufficient to induce pERK activity (green) in many transgene-positive neurons. Fish were food-deprived for 2 hours and then fed in the presence of whole-field 630 nm LED illumination (as in Figure 6). White arrows indicate examples of cells with higher pERK activity. Scale bar =20 μm. Insets (white boxes) are shown at higher magnification on the right. Width of insets = 40 μm.

(b) The pERK intensities of ReaChR-positive and -negative cells (normalized to the mean pERK intensity of ReaChR-negative cells for each fish) are plotted for 3 individual fish. To sample ReaChR-negative cells, all visible cells lacking red channel expression were selected in every 3rd to 5th z-plane (to minimize oversampling). Fish 1 corresponds to the fish in **(a).** Box plot indicates mean value (horizontal line), 1 SD (gray box) and 95% confidence intervals (vertical line). Individual cells are plotted as circles. In *Tg(y333:Gal4;UAS:ReaChR-RFP)* transgene-positive fish, ReaChR positive cells have significantly higher pERK fluorescence intensity, demonstrating the effectiveness of optogenetic activation ($p = 2.7x10^{-6}/2.7x10^{-8}/6.5x10^{-13}$ for each fish respectively, one-tailed Wilcoxon rank-sum test).

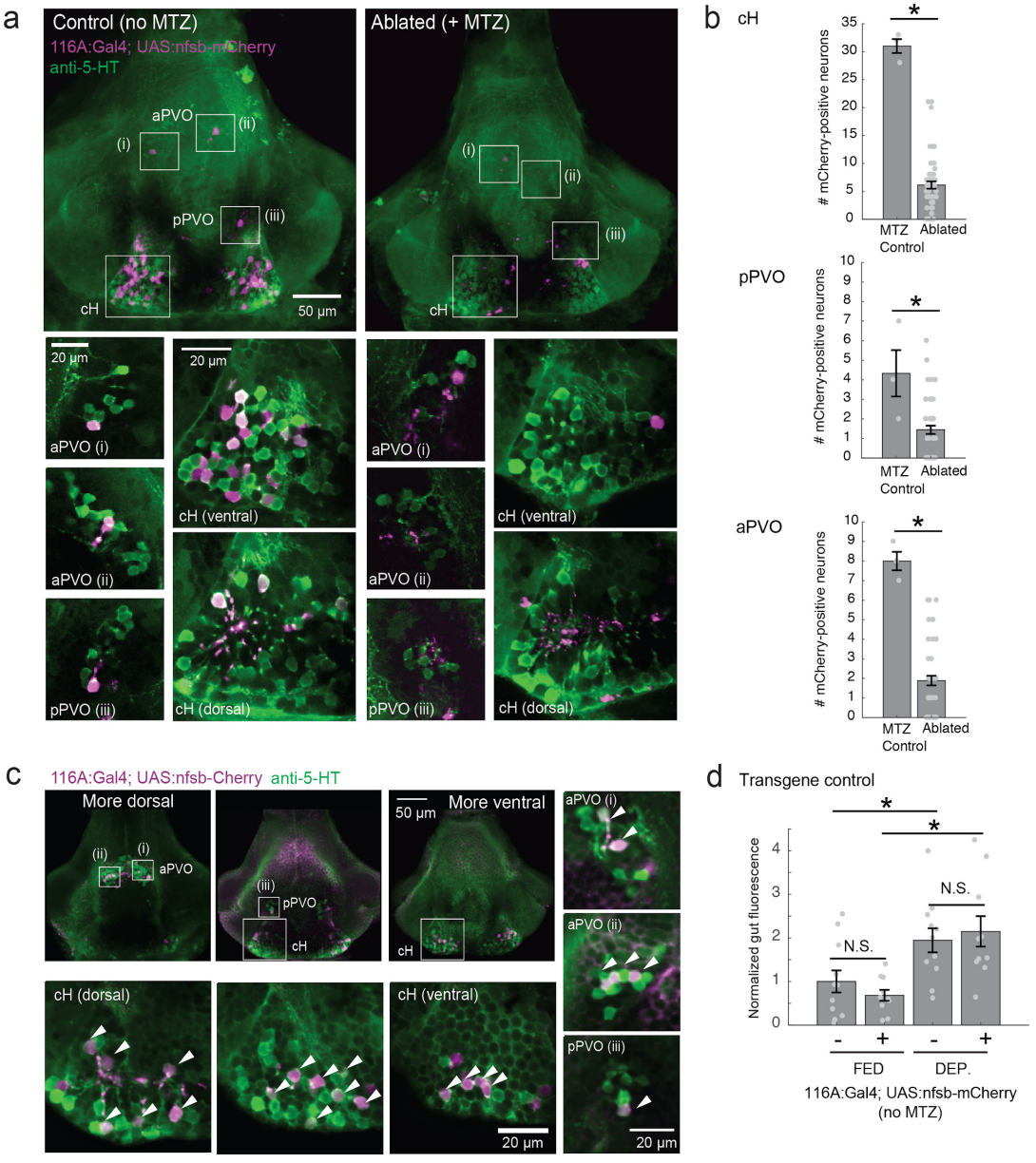

Figure 6 - Figure Supplement 2: Nitroreductase-mediated ablation of cH serotonergic neurons
(a) Ablation of *Tg(116A:Gal4;UAS:nfsb-mCherry)*-labeled neurons. Note that due to sparse expression of the transgenes, ablation of the cH/PVO populations is likely to be partial (<50%). Representative projection images are shown of non-ablated animals (left) and animals following exposure to the chemical MTZ (right, see Methods). Scale bar = 50 μm. Insets (white boxes) show the locations of higher-magnification single-plane images of transgene-labeled cH, aPVO and pPVO areas and neuronal overlap with 5-HT expression (anti-5-HT antibody staining, green color). Scale bar = 20 μm.
(b) Quantification of ablation. When *Tg(116A:Gal4;UAS:nfsb-mCherry)* fish were incubated with MTZ, we observed 6.1± 0.66 (mean ± SEM) mCherry-positive cells (n = 54 fish). When MTZ was omitted, 31 ± 1.5 cells were mCherry-positive (n = 3 fish). The reduction resulting from ablation was thus ~80% (p = 0.0019, one-tailed Wilcoxon rank-sum test). pPVO (4.3 ± 1.5 control vs 1.4 ± 0.2 ablated, p = 0.0162) and aPVO (8.0 ± 0.6 control vs 1.9 ± 0.3 ablated, p = 0.0015) cells were also affected. Some of the remaining mCherry-positive cells were dimly fluorescent and misshapen/deformed, indicating damage that might impair function.
(c) Similar to Tg(116A:Gal4;UAS:GFP) (Figure 2 - Figure Supplement 2), there is strong overlap of *Tg(116A:Gal4;UAS:nfsb-mCherry)* with anti-5-HT immunostaining (green color). Scale bar = 50 μm. Insets (white boxes) show higher-magnification single-plane images of cH, aPVO and pPVO labeling by this transgene and overlap with 5-HT expression. Scale bar = 20 μm.
(d) The *Tg(116A:Gal4;UAS:nfsb-mCherry)* transgene does not affect feeding in the absence of MTZ, relative to siblings lacking transgene expression. Fed: p = 0.64, n = 11(negative)/10(positive); Dep.: p = 0.91, n = 11(negative)/10(positive), Fed vs Dep.: p = 0.035(negative)/7.7×10^{-4}(positive).

DISCUSSION

Decades-old studies on appetite regulation in mammals have suggested that the hypothalamus consists of modular units that functionally interact to suppress or enhance food intake. Here we show that the larval zebrafish hypothalamic network can similarly be divided into medial and lateral units on the basis of neural activity and function. These units show anti-correlated activity patterns extending through various states and distinct behaviors during periods of food deprivation and feeding. We propose these states are analogous to those commonly referred to as hunger and satiety and reflect the animal's drive to maintain energy homeostasis (Figure 6d). Furthermore, we show that within these broad neural response classes lie subpopulations that encode specific stimuli and perform distinct functions depending on the timing of their activation.

Mutually opposing hypothalamic networks control zebrafish appetite

We show that the medial hypothalamic zone, especially the caudal hypothalamus (cH), is strongly activated by food-deprivation and silent during voracious feeding, and that these changes in activity occur on a timescale of seconds to minutes. Here, we focused mainly on the cH serotonergic neurons, although many medially localized neurons show similar activity

814 patterns. In contrast, the lateral hypothalamus (LH), which contains GABAergic and
815 glutamatergic neurons, can be inhibited by the cH (Figure 5) and is silent in the absence of food;
816 conversely it is most strongly active during voracious feeding when cH serotonergic neurons are
817 least active. Interestingly, fish that display satiated feeding behavior exhibit intermediate activity
818 levels in the two hypothalamic regions (Figure 1). Thus, larval zebrafish have a motivational
819 state dependent upon food deprivation (i.e. hunger), which is encoded by two alternative and
820 distinct states of activity in opposing brain regions, with restoration of energy homeostasis (i.e.
821 satiety) paralleled by an intermediate state of balanced activity.

822 While generally anti-correlated, the cH and LH also appear to be differentially modulated
823 by both internal energy states and external factors such as prey. In the absence of food, LH
824 neural activity decreases rapidly (Figure 2), suggesting a requirement of external food cues to
825 drive LH activity, though some modest rate of spontaneous activity is still observed (Figure 5,
826 Figure 3 - Figure Supplement 3). In contrast, the slower timescale of increasing cH activity
827 during food deprivation (Figure 2, Figure 3 - Figure supplement 3) may reflect a rising caloric
828 deficit. Notably, many of the cH neurons are cerebrospinal fluid-contacting and thus have
829 access to circulatory information (Lillesaar, 2011; Pérez et al., 2013).

830 When prey is presented to a food-deprived animal, a rapid state change occurs as LH
831 neural activity is strongly increased and cH activity rapidly diminishes (Figure 1-4). Importantly,
832 the silence of cH neurons and strength of LH activity were correlated with the extent of prior
833 food-deprivation (Figure 2), suggesting a role for these nuclei in regulating food intake based on
834 energy needs. Also, the relatively quick timescale of these changes in activity suggests that they
835 do not reflect a change in caloric deficit (i.e. a change in hunger state), which would take
836 significantly longer to be alleviated. Further, the striking anti-correlation between the cH and LH
837 is consistent with their mutual inhibition, and suggests that the acute reduction in cH activity
838 allows for rapid LH excitation upon the presentation of prey cues. We supported this notion by
839 showing that optogenetic stimulation of a subset of cH neurons could inhibit lLH activity (Figure

5). However, the mechanisms for cH and LH mutual interactions are still unknown. It is possible that the cH may act via nearby inhibitory GABAergic neurons, and/or exert its effects through direct secretion of monoamines into the ventricles or perineuronal space. However, the fast (seconds) anti-correlation between cH and LH calcium activity (Figure 3), suggests the presence of direct inhibitory connections. The LH, which was previously characterized in Muto et. al (2017), similarly does not appear to send direct projections to the cH, but could potentially interact via intermediary neurons in the medial/periventricular regions of the hypothalamus.

The cH and LH show differential sensitivity to prey sensory and consummatory cues

Ingestive behavior has been proposed to comprise a series of sequential phases: 1) the initiation phase, triggered by energy deficit, in which the animal begins to forage; 2) the procurement phases, triggered by the presence of food sensory cues, in which the animal seeks and pursues food; and 3) the consummatory phase, which usually involves more stereotyped motor programs (Berthoud, 2002; Watts, 2000). An animal's energy status is sensed internally and may influence the initiation, procurement and consummatory stages of ingestive behavior. Thus, a hungry animal will be more alert to food cues, seek food more persistently and also eat it more voraciously.

In mammals, LH neurons are responsive to both external food sensory cues and consummatory cues (Jennings et al., 2015). Here, we show that the LH lobes in zebrafish also respond differentially to food cues. In the "sensory" stage, the mLH and lLH are already activated, which may reflect an enhanced sensitivity to food cues during hunger. In contrast, cH activity transiently falls (as shown by calcium imaging in Figure 3) but remains overall high.

Notably, cH inhibition and LH activation during the sensory stage is not as strong as post-food consumption (Figure 4), which induces massive and opposing changes in the activity of both domains. Since LH and cH activity are modulated within minutes of food consumption, they are unlikely to reflect satiety signals, and rather might play a role in further driving

voracious food consumption, at least until the activity of both populations returns to baseline. While it is unclear which consummatory cues modulate LH and cH activity, based on live imaging results from Muto et al (2017), the greatest enhancement of LH activity was observed almost immediately (milliseconds to seconds) after paramecia consumption. Thus, the cue is likely a fast pregastric signal (taste/tactile/swallowing), rather than postgastric absorption or hormone secretion.

Finally, our data raises the possibility of functional compartmentalization within the LH. Especially in terms of cellular pERK activity, the lLH is more weakly activated by food sensory cues compared to the mLH, suggesting that the lLH, similar to the cH, may be more sensitive to consummatory cues than sensory food cues alone. These results are also consistent with a generally stronger anti-correlation of the lLH with cH activity (compared to mLH), as also observed in our calcium imaging and optogenetic experiments. Further molecular, cellular and functional dissection of the individual LH lobes will allow for a better understanding of their behavioral roles.

Functional roles of the cH and LH in and beyond appetite control

Finally, we test the hypothesis that the cH and LH form mutually antagonistic functional units that dominate different phases of hunger and drive appropriate behavioral responses during each phase (Figure 6). In particular, we show that the activation state of the cH is a crucial regulator of satiation-state dependent food intake. Artificial cH activation in satiated fish *prior* to feeding is sufficient to drive subsequent voracious feeding. Based on observed cH dynamics, we propose that the degree on cH inhibition during voracious feeding is proportional to the degree of cH activation prior to feeding. This could be mediated by the release of serotonin/other neuromodulators over the course of food-deprivation, which may be capable of sensitizing the LH even in the absence of food cues. In this way, zebrafish are able to retain a "memory" of their hunger state, which is released once food is presented. This motif might help ensure that the animal eventually returns to a stable equilibrium, that is, satiety.

We furthermore show that the acute effect of cH activation *during* feeding is suppression of food intake, whereas cH ablation enhances food intake, which is again consistent with mammalian studies of medial hypothalamic areas. At first glance, the observation that the cH acutely suppresses food intake is inconsistent with the idea that it is most active during hunger. However, the critical difference here is the presence or absence of food. Once food is presented to a hungry fish, high activity in the cH may simply suppress LH activity, and hence elevate the initial threshold for food intake.

The seemingly paradoxical roles of the cH during hunger may also make sense when considering that, in the absence of food, consummatory behavior would in fact be counterproductive. Thus, during food-deprivation, the cH may play complementary roles such as the sensitization of the LH and/or other feeding-related circuits (as discussed above), or drive alternative behavioral programs, like foraging or energy-conserving measures (see Supplementary File 1 - Conceptual Circuit Model for a more in-depth discussion). Given that cH neurons appear also to be activated by aversive stimuli (Randlett et al., 2015; Wee et al., 2019), they might quite generally encode a negative valence state, of which being hungry in the absence of food is an example. This then suggests that the silence of these neurons in a hungry fish where food is present implies a positive valence state, a notion that is in ready agreement with human subjective experience. Similar features of hunger-related (i.e. AgRP) neurons have also been described in mammals (Betley et al., 2015; Chen et al., 2015; Dietrich et al., 2015; Mandelblat-Cerf et al., 2015).

Although the cH does not have an exact mammalian homolog, its functions have been proposed to be adopted by other modulatory populations, such as the serotonergic raphe nucleus in mammals (Gaspar and Lillesaar, 2012; Lillesaar, 2011). While known to be a potent appetite suppressant, serotonin is also released during food deprivation, and has been shown to enhance food-seeking behavior (Elipot et al., 2013; Kantak et al., 1978; Pollock and Rowland, 1981; Voigt and Fink, 2015). Thus, our results showing opposing cH activity patterns during

hunger could reflect similarly complex roles of serotonin in zebrafish, potentially explaining some of its paradoxical functions. The cH and PVO also express dopaminergic (intermingled with 5-HT) and a much smaller fraction of histaminergic neurons, which appear to be densely interconnected (Chen et al., 2016; Kaslin and Panula, 2001). We note that our data, while confirming a role of serotonergic neurons, does not rule out an involvement of these other neuromodulators in appetite control, particularly dopamine.

Further, we do not rule out the involvement of other circuits in appetite control; in fact, there are likely numerous players involved. For example, the PVO appears to be modulated by food cues and food-deprivation, is anti-correlated with LH activity, and labeled by our transgenic lines (albeit more sparsely), suggesting it may complement the role of the cH. Our conclusions are also limited by the available tools and methodologies -- since different transgenic lines were utilized for stimulation and ablation, we cannot be certain that we are manipulating the same population of neurons, though both share mutual overlap with serotonergic cells. Also, due to the lack of complete transgene specificity, there is a possibility that our manipulations may affect non-specific targets such as the olfactory bulb.

The strong LH activation after food-deprivation suggests that this region is involved in the induction of voracious feeding. This notion is supported by Muto et al (2017) who recently demonstrated that inhibition of the LH impairs prey capture, a behavior that is clearly related to voracious feeding.. Furthermore, electrical stimulation of the homologous region (lateral recess nuclei) in adult cichlids and bluegills (Demski, 1973; Demski and Knigge, 1971) can elicit feeding behavior, which is consistent with our hypothesis. Interestingly, while stimulating some of these regions induced food intake, the activation of others induced behaviors such as the “snapping of gravel”, which are reminiscent of food search or procurement. In mammals, electrical or optogenetic stimulation of LH neurons triggers voracious eating, again consistent with our findings that the LH is highly activated during the voracious eating phase in hungry fish (Delgado and Anand, 1953). In particular, GABAergic neurons that do not co-express MCH or

Orexin have been shown to be responsive to food cues and are sufficient to stimulate food intake in mammals (Jennings et al., 2015). Whether these GABAergic and glutamatergic neurons of the zebrafish LH co-express other neuromodulators, as has been recently discovered in mammals (Mickelsen et al., 2019) remains to be explored. Overall, these data suggest that the zebrafish LH may play an important role in driving food intake during hunger, despite some differences in peptidergic expression from mammalian LH. Certainly, since cues such as water flow and optogenetic stimulation light are sufficient to modulate cH and/or LH neurons, these hypothalamic loci are likely also involved in other sensorimotor behaviors beyond appetite regulation.

In conclusion, we have shown here how anatomically segregated hypothalamic nuclei might interact to control energy homeostasis. We argue that the medial-lateral logic of hypothalamic function that is well established in mammalian systems may be conserved even in non-mammalian vertebrates, though their activity patterns may possibly be more complex than originally believed. Our data suggests diverse roles of neuromodulators such as serotonin in regulating behavioral responses during hunger, which may complement mammalian observations. Finally, we propose that investigating large-scale network dynamics may reveal an additional layer of insight into the principles underlying homeostatic behavior, which might be overlooked when studies are restricted to the observation and perturbation of smaller subpopulations.

SUPPLEMENTARY FIGURE LEGENDS

Supplementary Table 1: Z-brain anatomical regions that are more activated in voraciously feeding (food-deprived + food) fish as compared to fed fish.

Supplementary Table 2: Z-brain anatomical regions that are more activated in fed fish as compared to voraciously feeding (food-deprived + food) fish.

Video 1: Z-stack (dorsal to ventral) of brain activity map shown in Figure 1b.

Video 2: Z-stack (ventral to dorsal) of anti-5HT (green) and anti-pERK (magenta) staining in

975 food-deprived fish
976
977 **Video 3:** Z-stack (ventral to dorsal) of TH2:GCaMP5 transgene expression (green) and anti-
978 pERK (magenta) staining in the same food-deprived fish
979
980 **Video 4:** Video of larval zebrafish hunting artemia larvae. Prey-capture behavior, such as J-
981 bends and pursuits, but no capture swims, were observed in response to artemia larvae.
982 Recording rate: 30 fps. Playback rate: Real time.
983
984 **Supplementary File 1: Conceptual Circuit Model**
985 A comprehensive overview of our circuit model and current understanding, including a circuit
986 diagram, detailed elaboration and testable predictions.
987
988
989 **MATERIALS AND METHODS**
990
991 **Key Resource Table**

Reagent type (species) or resource	Designation	Source or reference	Identifiers	Additional information
genetic reagent *(danio rerio)*	*Tg(pGal4FF:116A)*	Characterized in this manuscript		Dr. Koichi Kawakami (NIG, Japan)
genetic reagent *(danio rerio)*	*Tg(pGal4FF:76A)*	PMID: 28425439		Dr. Koichi Kawakami (NIG, Japan)
genetic reagent *(danio rerio)*	*Tg(y333:Gal4)*	PMID: 26635538		Dr. Harold Burgess (NIH)
genetic reagent *(danio rerio)*	*Tg(HuC:GCaMP6s)*	PMID: 28892088		Dr. Florian Engert (Harvard)
genetic reagent *(danio rerio)*	*Tg(UAS:GCaMP6s)*	PMID: 28425439		Dr. Koichi Kawakami (NIG, Japan)
genetic reagent *(danio rerio)*	*Tg(UAS:ReaChR-RFP)*	Characterized in this manuscript		Dr. Misha Ahrens (Janelia Research Campus)
genetic reagent *(danio rerio)*	*Tg(UAS-E1b:NTR-mCherry)*	PMID: 17335798		Available from ZIRC

genetic reagent *(danio rerio)*	*Tg(Vglut2a:dsRed)*	PMID: 19369545		
genetic reagent *(danio rerio)*	*Tg(Gad1b:loxP-dsRed-loxP-GFP)*	PMID: 23946442		
genetic reagent *(danio rerio)*	*Tg(Gad1b:GFP)*	PMID: 23946442		
genetic reagent *(danio rerio)*	*Tg(TH2:GCamP5)*	PMID: 26774784		Dr. Adam Douglass (University of Utah)
genetic reagent *(danio rerio)*	*Tg(ETvmat2:GFP)*	PMID:18164283		
genetic reagent *(danio rerio)*	*Tg(HCRT:RFP)*	PMID: 25725064		
antibody	Rabbit monoclonal anti-pERK	Cell Signaling	4370 RRID:AB_2315112	IHC (1:500)
antibody	mouse monoclonal anti-ERK	Cell Signaling	4696 RRID:AB_390780	IHC (1:500)
antibody	rabbit polyclonal anti-5-HT	Sigma-Aldrich	S5545 RRID:AB_477522	IHC (1:500)
antibody	goat polyclonal anti-5-HT	AbCam	ab66047 RRID:AB_1142794	IHC (1:500), 2% BSA in PBS, 0.3% Triton blocking solution)
antibody	goat polyclonal anti-MSH	EMD Millipore	AB5087 RRID:AB_91683	IHC (1:500), 2% BSA in PBS, 0.3% Triton blocking solution)
antibody	rabbit polyclonal anti-AGRP	Phoenix Pharmaceuticals	H-003-53 RRID:AB_2313908	IHC (1:500)
antibody	rabbit polyclonal anti-MCH	Phoenix Pharmaceuticals	H-070-47 RRID:AB_10013632	IHC (1:500)
antibody	rabbit polyclonal anti-CART	Phoenix Pharmaceuticals	55-102 RRID:AB_2313614	IHC (1:500)

antibody	rabbit polyclonal anti-NPY	Immunostar	22940 RRID:AB_2307354	IHC (1:500)
antibody	mouse monoclonal anti-TH	Immunostar	22941 RRID:AB_1624244	IHC (1:500)
chemical compound, drug	DiD' solid (lipid dye)	Thermo Fisher Scientific	D-7757	Stock solution (10mg/ml), working solution (2.5mg/ml), in ethanol

Fish husbandry and transgenic lines

Larvae and adults were raised in facility water and maintained on a 14:10 hr light:dark cycle at 28°C. All protocols and procedures involving zebrafish were approved by the Harvard University/Faculty of Arts & Sciences Standing Committee on the Use of Animals in Research and Teaching (IACUC). WIK wildtype larvae and mit1fa-/- (nacre) larvae in the AB background, raised at a density of ~40 fish per 10 cm petri dish, were used for behavioral and MAP-mapping experiments.

Transgenic lines *Tg(UAS-E1b:NTR-mCherry)* (Davison et al., 2007) (referred to as UAS:nfsb-mCherry), *Tg(UAS:GCaMP6s)* (Muto and Kawakami, 2011; Muto et al., 2017) *Tg(HuC:GCaMP6s)* (Kim et al., 2017), *Tg(Vglut2a:dsRed)* (Miyasaka et al., 2009), *Tg(Gad1b:loxP-dsRed-loxP-GFP* and *Tg(Gad1b:GFP)* (Satou et al., 2013), *Tg(TH2:GCamP5)* (McPherson et al., 2016), *Tg(ETvmat2:GFP)* (referred to as VMAT:GFP) (Wen et al., 2008), *Tg(HCRT:RFP)* (Liu et al., 2015) have all been previously described and characterized. *Tg(pGal4FF:116A)* (referred to as 116A:Gal4) was isolated from a gene trap screen by the Kawakami group (Kawakami et al., 2010), *Tg(pGal4FF:76A)* was recently published by the same group (Muto et al., 2017) (Muto et al., 2017). *Tg(y333:Gal4)* from a different enhancer trap screen was used to drive expression in the cH in cases where 116A:Gal4-driven expression was sparse (Marquart et al., 2015) (Marquart et al., 2015). *Tg(UAS:ReaChR-RFP)* was generated by Chao-Tsung Yang (Ahrens lab, Janelia Research Campus) using Tol2 transgenesis. The same optogenetic channel was previously validated in zebrafish in Dunn et al., 2016.

MAP-mapping of appetite regions

More details on the MAP-mapping procedure can be found in Randlett et al (2015). 5-6 dpf, *mit1fa-/-* (nacre) larvae in the AB background larvae were fed an excess of paramecia once daily. On the day of the experiment (at 7 dpf), the larvae were distributed randomly into two treatment groups: 1) Food-deprived, where larvae were transferred into a clean petri dish of facility water, taking care to rinse out all remaining paramecia or 2) Fed, where after washing

and transferring they were fed again with an excess of paramecia. After two hours, larvae in both groups were fed with paramecia. After 15 minutes, larvae were quickly funneled through a fine-mesh sieve, and the sieve was then immediately dropped into ice-cold 4% paraformaldehyde (PFA) in PBS (PH 7.2-7.4). Fish were then immunostained with procedures as reported below (see Immunostaining methods). The rabbit anti-pERK antibody (Cell Signaling, #4370) and mouse anti-ERK (p44/42 MAPK (Erk1/2) (L34F12) (Cell Signaling, #4696) were used at a 1:500 dilution. Secondary antibodies conjugated with alexa-fluorophores (Life Technologies) were diluted 1:500. For imaging, fish were mounted dorsal-up in 2% (w/v) low melting agarose in PBS (Invitrogen) and imaged at ~0.8/0.8/2 µm voxel size (x/y/z) using an upright confocal microscope (Olympus FV1000), using a 20x 1.0NA water dipping objective. All fish to be analyzed in a MAP-Mapping experiment were mounted together on a single imaging dish, and imaged in a single run, alternating between treatment groups.

ICA analysis

ICA analysis was performed exactly as reported in Randlett et al, 2015. The central brain (not including eyes, ganglia, or olfactory epithelia) from each fish was downsampled into 4.7um^3 sized voxels to generate a pERK level vector for each fish. Fish in which any of the voxels was not imaged (due to incomplete coverage) were excluded from the analysis. Fish were normalized for overall brightness by dividing by the 10th percentile intensity value, and voxels normalized by subtracting the mean value across fish. The fish-by-voxel array was then analyzed for spatially independent components using FastICA (http://research.ics.aalto.fi/ica/fastica/, Version 2.5), treating each fish as a signal and each voxel as sample, using the symmetric approach, 'pow3' nonlinearity, retaining the first 30 principal components and calculating 30 independent components. Independent component (IC) maps are displayed as the z-score values of the IC signals.

Since ICA analysis requires a substantial sample size, the original analysis reported in Randlett et al (2015) included 820 fish exposed to various treatments, including fish sampled at different points of the day and night, and fish given various noxious or food stimuli, additional fish stimulated with electric shocks, light flashes, moving gratings, heat, mustard oil, melatonin, clonidine, nicotine, cocaine, ethanol and d-amphetamine.

Here, to focus the analysis on more naturalistic feeding conditions, we restricted the dataset to n = 300 fish that were either food-deprived (2 hrs), or presented with food in food-deprived or fed conditions.

Whole-mount Immunostaining

24 hours after fixation (4% paraformaldehyde (PFA) in PBS), fish were washed in PBS + 0.25% Triton (PBT), incubated in 150mM Tris-HCl at pH 9 for 15 min at 70°C (antigen retrieval), washed in PBT, permeabilized in 0.05% Trypsin-EDTA for 45 min on ice, washed in PBT, blocked in blocking solution (10% Goat Serum, 0.3% Triton in BSS or 2% BSA in PBS, 0.3% Triton) for at least an hour and then incubated in primary and secondary antibodies for up to 3 days at 4°C diluted in blocking solution. In-between primary and secondary antibodies, fish were washed in PBT and blocked for an hour. If necessary, pigmented embryos were bleached for 5 min after fixation with a 5%KOH/3%H2O2 solution.

The protocol was similar for dissected brains, except that the brains were dissected in PBS after 24 hours of fixation, and the Tris-HCL antigen retrieval/permeabilization step in Trypsin-EDTA was omitted. Dissected brains were mounted ventral up on slides in 70% glycerol prior to imaging. Confocal images of dissected brains were obtained using either a Zeiss LSM 700 or Olympus FV1000.

Quantification of food intake

Paramecia cultures (~1-2 500 ml bottles) were harvested, spun down gently (<3000 rpm) and concentrated, and subsequently incubated with lipid dye (DiD' solid, D-7757, Thermo Fisher Scientific, dissolved in ethanol) for > 2 hrs (5 µl of 2.5mg/ml working solution per 1 ml of concentrated paramecia) on a rotator with mild agitation. They were then spun down gently (<3000 rpm), rinsed and reconstituted in deionized water. An equal amount (100µl, ~500 paramecia) was pipetted into each 10 cm dish of larvae. This method was adapted from Shimada et al., 2012. After the experiment, larvae were fixed and mounted on their sides on glass slides or placed in wells of a 96 well plate. They were then imaged using the AxioZoom V16 (Zeiss) and analyzed using custom Fiji (Schindelin et al., 2012) software. In cases where the identity of larvae needed to be maintained, for example, to correlate food intake with brain activity, larvae were imaged and subsequently stained individually in 96 well plates. This led to more variable staining which affects analysis of mean fluorescence.

Larvae were always distributed randomly into experimental groups.

Quantification of LH and cH activity in dissected brains

Brains within each dataset were usually registered onto a selected reference image from the same dataset using the same CMTK registration software used in MAP-mapping. Further analysis was then performed using custom Fiji and MATLAB software.

For quantification of cH, mLH and pERK fluorescence intensity, ROIs were manually defined using the reference image, and pERK intensity was quantified over all registered images and averaged across the entire lobe (multiple z-planes) as well as across both lobes. Analysis of cH pERK fluorescence was restricted to the most ventral planes, as more dorsal cH neurons show weaker correlation with feeding states (e.g. Figure 1 - Figure Supplement 5).

For quantification of mLH and lLH active cell count, automated analysis of cell count was again performed using custom Fiji software, namely: 1) Image processing to reduce background and enhance contrast 2) Adaptive thresholding to isolate strongly-stained cells 3) Applying the "Analyze Particles" function to quantify the number of cells within each manually-defined ROI.

Aggregation and visualization of results was performed using custom MATLAB software.

Note that, in experiments in which the data was collected without the tERK channel (e.g. from Figure 2), thus prohibiting image registration, ROIs were drawn manually over each region

across all z-planes and averaged to obtain mean fluorescence values.

For Figure 2 - Figure Supplement 1, where individual fish were stained, all measurements, including cell count, were made manually. In addition, background fluorescence was measured for each sample and subtracted from measured values.

Semi-automated quantification of ReaChR overlap with pERK

This section describes the analysis method for Figure 6 - Figure Supplement 1. The multi-point picker on ImageJ was first used to select all visible 5-HT, ReaChR-positive or ReaChR-negative cells within each z-stack for each fish. A custom Fiji macro was then used to extract mean pERK intensities from all identified cells, and data was further processed using MATLAB. Data was plotted using the notBoxPlot.m Matlab function.

Calcium imaging

For confocal calcium imaging of the cH and LH simultaneously in the presence of food, *Tg(76A:Gal4;116A:Gal4; UAS:GCaMP6s)* triple transgenic fish were embedded in 1.8% agarose, with their eyes/nostrils were released. GCaMP activity from a single z-plane (where the cH and LH neurons could be seen) was imaged using a confocal microscope (Olympus FV1000) at 1 fps. After a 5 min habituation period and a 10 min baseline period, a dense drop of paramecia was pipetted into the dish. Due to paramecia phototaxis, most of the paramecia moved into close vicinity of the fish's head under the laser, allowing for strong visual/olfactory exposure to paramecia. After image registration (TurboReg Fiji Plugin, Thevenaz et al., 1998), and downsampling (Fiji/MATLAB), manually-segmented ROIs were selected and total fluorescence within the ROI was calculated. Cross-correlation and other analyses were performed using custom MATLAB software.

For long-term 2P imaging of the cH and LH simultaneously in the absence of food (Figure 3 - Figure Supplement 3), *Tg(76A:Gal4;116A:Gal4; UAS:GCaMP6s)* triple transgenic fish were embedded in 1.8% agarose. GCaMP activity from either multiple slices (3 z-planes spanning a ~20 μm volume of the intermediate hypothalamus using an electrically-tunable liquid lens (Edmund Optics, 83-922), 237 ms per z-plane) or a single z-plane where the cH and LH neurons (1.5 fps) could be seen was imaged using custom 2P microscopes. After image registration and downsampling to cell-sized voxels (Fiji/MATLAB), manually segmented ROIs were selected and total fluorescence within the ROI was calculated. Clustering, spike detection and other analyses were performed using custom MATLAB software. Baseline detrending was performed on "raw" Δf/f traces by fitting a quadratic polynomial and subtracting it from the trace. Calculations on spike frequency and amplitude were subsequently performed using baseline-detrended calcium traces.

Optogenetic stimulation and simultaneous calcium imaging

Optogenetic stimulation and calcium imaging was performed on a confocal microscope (Zeiss LSM 880) using a 633 nm laser for ReaChR activation, and a 488 nm laser for calcium imaging.

Tg(y333:Gal4;UAS:ReaChR-RFP; HuCGCaMP6s) triple-transgenic fish were used to record LH activity after ReaChR activation. As *Tg(HuC:GCaMP6)* does not label the cH, in some cases we used fish that also had *Tg(UAS:GCaMP6s)* co-expressed in cH, allowing for monitoring of cH activity directly.

The ReaChR activation spectrum is wide and 488 nm laser power at sufficiently high intensities is sufficient to activate ReaChR. Since *Tg(y333:Gal4;UASGCaMP6s)* is expressed strongly in the cH, weak 488 nm laser power can be used to monitor cH activity after ReaChR activation of cH. On the other hand, *Tg(HuC:GCaMP6s)* expression in the LH is considerably weaker than *Tg(UAS:GCaMP6s)* expression driven by *Tg(y333:Gal4)*, and recording LH activity requires high laser power. Thus, during LH recording trials, we could not simultaneously image the cH.

Fed fish were embedded in 1.8%-2% agarose, with tails, mouth and eyes freed, 15-20 minutes before imaging in the absence of food. For baseline recording, spontaneous activities in cH or LH were recorded. ReachR activation was then induced in one side of cH periodically for 10-15 s, and ensuing activity in one or both sides of LH or cH was recorded continuously during intervals (of 120-180 s) between stimuli.

Nitroreductase-mediated ablations

Larvae expressing *Tg(116A:Gal4;UAS:nfsb-mCherry)*, or their non-transgenic siblings were incubated in 2.5 mM Metronidazole (Sigma-Aldrich, M3761) from 4-6 dpf/5-7 dpf. MTZ was subsequently washed out, and food intake was measured at 7 or 8 dpf. For these experiments, the MTZ-treated non-transgenic siblings were used as the control group. Each control or ablated group was food-deprived or fed for 2 hrs, and labeled food was added to quantify food intake. In the case of fed fish, unlabeled food was very gently washed out 15 mins before the experiment and the food-deprived fish were also agitated slightly to simulate a short washout.

Optogenetic stimulation with behavior

Optogenetic stimulation was done by placing a square LED panel (630 nm, 0.12mW/mm^2 driven at full current, Soda Vision, Singapore) directly on top of petri dishes containing ReaChR positive or negative fish, for 10 minutes continuously before or during feeding. We had attempted other methods of stimulating the fish (e.g. pulsed LED stimulation) but found that it was disruptive to behavior.

Artemia Hunting Video

7 dpf larval fish were food-deprived for 2 hours, acclimatized in 24 well plates for 30 minutes, and then fed either an excess of hatched artemia or paramecia. Raw videos of hunting behavior were then recorded for 10 min at 30 fps using a high-resolution monochrome camera (Basler acA4924) and custom Python-based acquisition software.

High-resolution behavioral tracking

We developed a system (Johnson et al., 2019) in which a high-speed infrared camera moves on motorized rails to automatically track a zebrafish larvae in a large pool (300 x 300 x 4mm). A single fish is recruited to the arena center with motion cues delivered from a projector to initiate each trial. Paramecia are dispersed throughout the middle of the pool For analysis 60 Hz image frames are centered and aligned. In every frame, the tail was skeletonized and the gaze angle of each eye is calculated. The eyes can each move from around zero degrees (parallel to body-axis) to 40 degrees (converged for hunting). Each bout was then represented as a point in 220-dimensional posture space by accumulating 22 posture measurements (20 tail tangent angles to encode tail shape, and 2 eye gaze angles) across 10 image frames (~167 ms) from the beginning of each bout. All bouts were then mapped to a 2-D space with t-distributed stochastic neighbor embedding (t-SNE), Four major hunting bout types can be identified from this embedding. Hunts begin with the “j-turn”, and fish follow and advance toward prey objects with “pursuit” bouts. Hunts end with an “abort” or a “strike”. When the fish is not actively involved in a hunt, it explores the arena with “exploratory” bouts. Fractions of hunting bouts were then compared between fed and food-deprived fish in 3-minute time bins over 45 min.

Statistics

All error bars show mean ± SEM over fish. Significance was reported as follows: *p<0.05. Significance was determined using the non-parametric Wilcoxon signed-rank test for paired data and the Wilcoxon rank-sum test for independent samples. One-tailed tests were performed in cases where there was a prior prediction regarding the direction of change. A one-or two-way ANOVA (Tukey-Kramer correction, MATLAB statistical toolbox) was used in cases where multiple comparisons were involved.

Code availability

Analysis code used in this manuscript is available on www.github.com/carolinewee

ACKNOWLEDGEMENTS

We thank Harold Burgess for kindly providing the y333:Gal4 transgenic line, and Adam Douglass who provided us with the TH2:GCaMP5 transgenic line. We further thank Thomas Panier who assisted Robert Johnson in construction of the rig used for high resolution behavioral imaging. Support from Steve Turney and the CBS imaging facility, and the Harvard Center for Biological Imaging were essential for the successful completion of many experiments. Finally, we would like to thank Jessica Miller, Steve Zimmerman, Karen Hurley and Brittany Hughes at Harvard for providing invaluable fish care.

COMPETING INTERESTS

The authors declare no competing interests.

REFERENCES

Ahima, R.S., and Antwi, D.A. (2008). Brain regulation of appetite and satiety. Endocrinol. Metab. Clin. North Am. *37*, 811–823.

Ammar, A.A., Södersten, P., and Johnson, A.E. (2001). Locus coeruleus noradrenergic lesions attenuate intraoral intake. Neuroreport *12*, 3095–3099.

Anand, B.K., and Brobeck, J.R. (1951). Hypothalamic control of food intake in rats and cats. Yale J. Biol. Med. *24*, 123–140.

Berridge, M.J. (1998). Neuronal calcium signaling. Neuron *21*, 13–26.

Berthoud, H.-R. (2002). Multiple neural systems controlling food intake and body weight. Neurosci. Biobehav. Rev. *26*, 393–428.

Betley, J.N., Xu, S., Cao, Z.F.H., Gong, R., Magnus, C.J., Yu, Y., and Sternson, S.M. (2015). Neurons for hunger and thirst transmit a negative-valence teaching signal. Nature *521*, 180–185.

Bianco, I.H., and Engert, F. (2015). Visuomotor Transformations Underlying Hunting Behavior in Zebrafish. Curr. Biol. *25*, 831–846.

Bianco, I.H., Kampff, A.R., and Engert, F. (2011). Prey capture behavior evoked by simple visual stimuli in larval zebrafish. Front. Syst. Neurosci. *5*, 101.

Brobeck, J.R., Larsson, S., and Reyes, E. (1956). A study of the electrical activity of the hypothalamic feeding mechanism. J. Physiol. *132*, 358–364.

Chen, Y.-C., Semenova, S., Rozov, S., Sundvik, M., Bonkowsky, J.L., and Panula, P. (2016). A Novel Developmental Role for Dopaminergic Signaling to Specify Hypothalamic Neurotransmitter Identity. J. Biol. Chem. *291*, 21880–21892.

Chen, Y., Lin, Y.-C., Kuo, T.-W., and Knight, Z.A. (2015). Sensory Detection of Food Rapidly Modulates Arcuate Feeding Circuits. Cell *160*, 829–841.

Curado, S., Stainier, D.Y., and Anderson, R.M. (2008). Nitroreductase-mediated cell/tissue ablation in zebrafish: a spatially and temporally controlled ablation method with applications in developmental and regeneration studies. Nat. Protoc. *3*, 948–954.

Davison, J.M., Akitake, C.M., Goll, M.G., Rhee, J.M., Gosse, N., Baier, H., Halpern, M.E., Leach, S.D., and Parsons, M.J. (2007). Transactivation from Gal4-VP16 transgenic insertions for tissue-specific cell labeling and ablation in zebrafish. Dev. Biol. *304*, 811–824.

Delgado, J.M.R., and Anand, B.K. (1953). Increase of food intake induced by electrical stimulation of the lateral hypothalamus. Am. J. Physiol. *172*, 162–168.

Demski, L.S. (1973). Feeding and aggressive behavior evoked by hypothalamic stimulation in a cichlid fish. Comp. Biochem. Physiol. Part A Physiol. *44*, 685–692.

Demski, L.S., and Knigge, K.M. (1971). The telencephalon and hypothalamus of the bluegill (Lepomis macrochirus): evoked feeding, aggressive and reproductive behavior with representative frontal sections. J. Comp. Neurol. *143*, 1–16.

Dietrich, M.O., Zimmer, M.R., Bober, J., and Horvath, T.L. (2015). Hypothalamic Agrp neurons drive stereotypic behaviors beyond feeding. Cell *160*, 1222–1232.

Dockray, G.J. (2009). The versatility of the vagus. Physiol. Behav. *97*, 531–536.

Dunn, T.W., Gebhardt, C., Naumann, E.A., Riegler, C., Ahrens, M.B., Engert, F., and Del Bene, F. (2016). Neural Circuits Underlying Visually Evoked Escapes in Larval Zebrafish. Neuron *89*, 613–628.

Elipot, Y., Hinaux, H., Callebert, J., and Rétaux, S. (2013). Evolutionary shift from fighting to foraging in blind cavefish through changes in the serotonin network. Curr. Biol. *23*, 1–10.

Fernandes, A.M., Fero, K., Arrenberg, A.B., Bergeron, S.A., Driever, W., and Burgess, H.A. (2012). Deep Brain Photoreceptors Control Light-Seeking Behavior in Zebrafish Larvae. Curr. Biol. *22*, 2042–2047.

Filosa, A., Barker, A.J., Dal Maschio, M., and Baier, H. (2016). Feeding State Modulates Behavioral Choice and Processing of Prey Stimuli in the Zebrafish Tectum. Neuron *90*, 596–

608.
Gaspar, P., and Lillesaar, C. (2012). Probing the diversity of serotonin neurons. Philos. Trans. R. Soc. Lond. B. Biol. Sci. *367*, 2382–2394.
Hoebel, B.G. (1965). Hypothalamic Lesions by Electrocauterization: Disinhibition of Feeding and Self-Stimulation. Science *149*, 452–453.
Jennings, J.H., Ung, R.L., Resendez, S.L., Stamatakis, A.M., Taylor, J.G., Huang, J., Veleta, K., Kantak, P.A., Aita, M., Shilling-Scrivo, K., et al. (2015). Visualizing Hypothalamic Network Dynamics for Appetitive and Consummatory Behaviors. Cell *160*, 516–527.
Johnson, R.E., Linderman, S., Panier, T., Wee, C.L., Song, E., Herrera, K.J., Miller, A., and Engert, F. (2019). Probabilistic Models of Larval Zebrafish Behavior: Structure on Many Scales. BioRxiv 672246.
Jordi, J., Guggiana-Nilo, D., Soucy, E., Song, E.Y., Wee, C.L., and Engert, F. (2015). A high-throughput assay for quantifying appetite and digestive dynamics. Am. J. Physiol. Regul. Integr. Comp. Physiol. ajpregu.00225.2015.
Jordi, J., Guggiana-Nilo, D., Bolton, A.D., Prabha, S., Ballotti, K., Herrera, K., Rennekamp, A.J., Peterson, R.T., Lutz, T.A., and Engert, F. (2018). High-throughput screening for selective appetite modulators: A multibehavioral and translational drug discovery strategy. Sci. Adv. *4*, eaav1966.
Kantak, K.M., Wayner, M.J., and Stein, J.M. (1978). Effects of various periods of food deprivation on serotonin turnover in the lateral hypothalamus. Pharmacol. Biochem. Behav. *9*, 529–534.
Kaslin, J., and Panula, P. (2001). Comparative anatomy of the histaminergic and other aminergic systems in zebrafish (Danio rerio). J. Comp. Neurol. *440*, 342–377.
Kawakami, K., Abe, G., Asada, T., Asakawa, K., Fukuda, R., Ito, A., Lal, P., Mouri, N., Muto, A., Suster, M.L., et al. (2010). zTrap: zebrafish gene trap and enhancer trap database. BMC Dev. Biol. *10*, 105.
Kim, D.H., Kim, J., Marques, J.C., Grama, A., Hildebrand, D.G.C., Gu, W., Li, J.M., and Robson, D.N. (2017). Pan-neuronal calcium imaging with cellular resolution in freely swimming zebrafish. Nat. Methods *14*, 1107–1114.
Krasne, F.B. (1962). General Disruption Resulting from Electrical Stimulus of Ventromedial Hypothalamus. Science *138*, 822–823.
Lillesaar, C. (2011). The serotonergic system in fish. J. Chem. Neuroanat. *41*, 294–308.
Lin, J.Y., Knutsen, P.M., Muller, A., Kleinfeld, D., and Tsien, R.Y. (2013). ReaChR: a red-shifted variant of channelrhodopsin enables deep transcranial optogenetic excitation. Nat. Neurosci. *16*, 1499–1508.
Liu, J., Merkle, F.T., Gandhi, A. V, Gagnon, J.A., Woods, I.G., Chiu, C.N., Shimogori, T., Schier, A.F., and Prober, D.A. (2015). Evolutionarily conserved regulation of hypocretin neuron specification by Lhx9. Development *142*, 1113–1124.
Mandelblat-Cerf, Y., Ramesh, R.N., Burgess, C.R., Patella, P., Yang, Z., Lowell, B.B., and Andermann, M.L. (2015). Arcuate hypothalamic AgRP and putative POMC neurons show opposite changes in spiking across multiple timescales. Elife *4*, e07122.
Marquart, G.D., Tabor, K.M., Brown, M., Strykowski, J.L., Varshney, G.K., LaFave, M.C., Mueller, T., Burgess, S.M., Higashijima, S., and Burgess, H.A. (2015). A 3D Searchable Database of Transgenic Zebrafish Gal4 and Cre Lines for Functional Neuroanatomy Studies. Front. Neural Circuits *9*, 78.
McPherson, A.D., Barrios, J.P., Luks-Morgan, S.J., Manfredi, J.P., Bonkowsky, J.L., Douglass, A.D., and Dorsky, R.I. (2016). Motor Behavior Mediated by Continuously Generated Dopaminergic Neurons in the Zebrafish Hypothalamus Recovers after Cell Ablation. Curr. Biol. *26*, 263–269.
Mickelsen, L.E., Bolisetty, M., Chimileski, B.R., Fujita, A., Beltrami, E.J., Costanzo, J.T., Naparstek, J.R., Robson, P., and Jackson, A.C. (2019). Single-cell transcriptomic analysis of

1348 the lateral hypothalamic area reveals molecularly distinct populations of inhibitory and excitatory
1349 neurons. Nat. Neurosci. *22*, 642–656.
1350 Miyasaka, N., Morimoto, K., Tsubokawa, T., Higashijima, S., Okamoto, H., and Yoshihara, Y.
1351 (2009). From the olfactory bulb to higher brain centers: genetic visualization of secondary
1352 olfactory pathways in zebrafish. J. Neurosci. *29*, 4756–4767.
1353 Muto, A., and Kawakami, K. (2011). Imaging functional neural circuits in zebrafish with a new
1354 GCaMP and the Gal4FF-UAS system. Commun. Integr. Biol. *4*, 566–568.
1355 Muto, A., Lal, P., Ailani, D., Abe, G., Itoh, M., and Kawakami, K. (2017). Activation of the
1356 hypothalamic feeding centre upon visual prey detection. Nat. Commun. *8*, 15029.
1357 Pérez, M.R., Pellegrini, E., Cano-Nicolau, J., Gueguen, M.-M., Menouer-Le Guillou, D., Merot,
1358 Y., Vaillant, C., Somoza, G.M., and Kah, O. (2013). Relationships between radial glial
1359 progenitors and 5-HT neurons in the paraventricular organ of adult zebrafish - potential effects
1360 of serotonin on adult neurogenesis. Eur. J. Neurosci. *38*, 3292–3301.
1361 Pisharath, H., and Parsons, M.J. (2009). Nitroreductase-Mediated Cell Ablation in Transgenic
1362 Zebrafish Embryos. In Methods in Molecular Biology (Clifton, N.J.), pp. 133–143.
1363 Pollock, J.D., and Rowland, N. (1981). Peripherally administered serotonin decreases food
1364 intake in rats. Pharmacol. Biochem. Behav. *15*, 179–183.
1365 Randlett, O., Wee, C.L., Naumann, E.A., Nnaemeka, O., Schoppik, D., Fitzgerald, J.E.,
1366 Portugues, R., Lacoste, A.M.B., Riegler, C., Engert, F., et al. (2015). Whole-brain activity
1367 mapping onto a zebrafish brain atlas. Nat. Methods *12*, 1039–1046.
1368 Satou, C., Kimura, Y., Hirata, H., Suster, M.L., Kawakami, K., and Higashijima, S. (2013).
1369 Transgenic tools to characterize neuronal properties of discrete populations of zebrafish
1370 neurons. Development *140*, 3927–3931.
1371 Schindelin, J., Arganda-Carreras, I., Frise, E., Kaynig, V., Longair, M., Pietzsch, T., Preibisch,
1372 S., Rueden, C., Saalfeld, S., Schmid, B., et al. (2012). Fiji: an open-source platform for
1373 biological-image analysis. Nat. Methods *9*, 676–682.
1374 Semmelhack, J.L., Donovan, J.C., Thiele, T.R., Kuehn, E., Laurell, E., and Baier, H. (2015). A
1375 dedicated visual pathway for prey detection in larval zebrafish. Elife *4*.
1376 Shimada, Y., Hirano, M., Nishimura, Y., and Tanaka, T. (2012). A high-throughput fluorescence-
1377 based assay system for appetite-regulating gene and drug screening. PLoS One *7*, e52549.
1378 Sternson, S.M., and Eiselt, A.-K. (2017). Three Pillars for the Neural Control of Appetite. Annu.
1379 Rev. Physiol. *79*, 401–423.
1380 Stuber, G.D., and Wise, R.A. (2016). Lateral hypothalamic circuits for feeding and reward. Nat.
1381 Neurosci. *19*, 198–205.
1382 Teitelbaum, P., and Epstein, A.N. (1962). The lateral hypothalamic syndrome: recovery of
1383 feeding and drinking after lateral hypothalamic lesions. Psychol. Rev. *69*, 74–90.
1384 Trivedi, C.A., and Bollmann, J.H. (2013). Visually driven chaining of elementary swim patterns
1385 into a goal-directed motor sequence: a virtual reality study of zebrafish prey capture. Front.
1386 Neural Circuits *7*, 86.
1387 Verkhratsky, A. (2005). Physiology and Pathophysiology of the Calcium Store in the
1388 Endoplasmic Reticulum of Neurons. Physiol. Rev. *85*, 201–279.
1389 Voigt, J.-P., and Fink, H. (2015). Serotonin controlling feeding and satiety. Behav. Brain Res.
1390 *277*, 14–31.
1391 Watts, A.G. (2000). Understanding the neural control of ingestive behaviors: helping to separate
1392 cause from effect with dehydration-associated anorexia. Horm. Behav. *37*, 261–283.
1393 Wee, C.L., Nikitchenko, M., Wang, W.-C., Luks-Morgan, S.J., Song, E., Gagnon, J.A., Randlett,
1394 O., Bianco, I.H., Lacoste, A.M.B., Glushenkova, E., et al. (2019). Zebrafish oxytocin neurons
1395 drive nocifensive behavior via brainstem premotor targets. Nat. Neurosci. *22*, 1477–1492.
1396 Wen, L., Wei, W., Gu, W., Huang, P., Ren, X., Zhang, Z., Zhu, Z., Lin, S., and Zhang, B. (2008).
1397 Visualization of monoaminergic neurons and neurotoxicity of MPTP in live transgenic zebrafish.
1398 Dev. Biol. *314*, 84–92.

Zhu, J.-N., and Wang, J.-J. (2008). The cerebellum in feeding control: possible function and mechanism. Cell. Mol. Neurobiol. *28*, 469–478.